

# Risk stratification of soft tissue sarcoma based on activity of prognostic molecules associated with unpolarized macrophages

Muhammad Usman<sup>1,2</sup>, Shengfa Lin<sup>3</sup>, Guiqiong He<sup>4\*</sup>, Hong Lu<sup>5\*</sup>

<sup>1</sup>Department of Anatomy, Institute of Neuroscience, Basic Medical College, Chongqing Medical University, Chongqing, China

<sup>2</sup>Department of Plastic Surgery, Central Hospital Affiliated to Chongqing University of Technology, Chongqing, China

<sup>3</sup>Department of Oncology, Jinshazhou Hospital of Guangzhou University of Chinese Medicine, Guangzhou, China

<sup>4</sup>Department of Anatomy, Institute of Neuroscience, Basic Medical College, Chongqing Medical University, Chongqing, China

<sup>5</sup>Department of Radiology, Central Hospital Affiliated to Chongqing University of Technology, Chongqing, China

**Submitted:** 31 August 2024; **Accepted:** 1 January 2025

**Online publication:** 13 February 2025

Arch Med Sci

DOI: <https://doi.org/10.5114/aoms/199702>

Copyright © 2025 Termedia & Banach

**\*Corresponding authors:**

Hong Lu

Department of Radiology

Central Hospital

Affiliated to

Chongqing University

of Technology

Chongqing, China

E-mail: 471739847@qq.com

Guiqiong He

Department of Anatomy

Institute of Neuroscience

Basic Medical College

Chongqing Medical

University

Chongqing, China

E-mail: [guiqionghe@cqmu.edu.cn](mailto:guiqionghe@cqmu.edu.cn)

edu.cn

## Abstract

**Introduction:** Soft tissue sarcomas (STS), representing 80% of sarcomas, are a rare and diverse group of neoplasms with a dire prognosis. Macrophages and their subtypes play an essential role with diverse outcomes in the tumor microenvironment (TME) of cancers, including sarcomas. The aim of this study was to investigate the role of macrophages in the development and prognosis of sarcoma patients.

**Material and methods:** Transcriptomic data from 5 sarcoma cohorts including 581 patients and transcripts of 56,752 single cells from 6 sarcoma patients were retrieved from public databases and analyzed. The infiltration of immune cells in the TME was evaluated with the CIBERSORT algorithm. Kaplan-Meier estimation with the log-rank test and Cox regression hazards models were adopted for evaluation of prognostic impacts.

**Results:** Deconvolution of 22 types of immune cells via the CIBERSORT algorithm revealed macrophages as a prominent component of the TME of sarcoma patients. Of these, M0 was associated with worst prognosis. A six-gene prognostic signature, termed MRPS, was developed that was significantly positively correlated with M0 macrophages. The MRPS-stratified high-risk subgroup showed abundance of M0 macrophages, indicating inhibition of macrophage polarization, specifically the classically activated pro-inflammatory M1 phenotype. Moreover, enrichment of oncogenic pathways and glycolysis and high frequency of mutations were evident. The robustness of the MRPS as a predictive biomarker was validated in external soft-tissue sarcoma patient datasets. A nomogram based on MRPS was developed as a potentially accurate and practical predictive tool for identifying high-risk sarcoma patients with lower survival probabilities. Furthermore, the MRPS signature exhibited reliable predictive capabilities for immunotherapy response, suggesting its potential to enhance the effectiveness of personalized immunotherapy in sarcoma patients.

**Conclusions:** MRPS represents a robust biomarker for predicting outcomes and response to therapy in soft-tissue sarcoma patients.

**Key words:** sarcoma, risk, CIBERSORT, biomarker, tumor microenvironment.

## Introduction

Sarcomas, comprising only 1% of adult malignancies, represent a rare and diverse group of neoplasms originating from mesenchymal tissues [1]. Heterogeneity is evident from the fact that sarcomas encompasses over 100 subtypes, each displaying variations in clinicopathological features, molecular characteristics, and responsiveness to treatment [1]. Categorized by the primary tissue of tumor origin, sarcomas consist of 80% soft tissue sarcoma (STS), 15% arising from bone tissue, and 5% classified as gastrointestinal stromal tumors (GISTs) [2]. STS itself comprises over 50 different neoplasms arising from various soft tissues including adipose and fibrous tissue, synovium, smooth and skeletal muscles, blood and lymphatic vessels, and peripheral nerves [1]. In the United States in 2023, there were an estimated 13,400 new cases and 5140 deaths due to cancers originating from soft tissues [3].

Surgical resection stands as the primary approach for treating STS, complemented by radiotherapy at various stages of the treatment process (pre-, intra-, and post-operatively, as well as concurrently with chemotherapy) [4]. However, the substantial heterogeneity of STS poses challenges, leading to variable responses to conventional treatments with limited applicability across subtypes [1, 5]. Notably, approximately one-third of sarcoma diagnoses progress to metastasis, exhibiting poor responsiveness to chemotherapy, typically the frontline treatment for advanced and metastatic cases [5]. Additionally, recurrence rates are markedly high, reaching about 20% [5]. Consequently, the 5-year survival rate for localized STS is about 50%, while for metastatic STS, it remains below 10% [6, 7].

In recent years, the role of tumor microenvironment (TME) components in cancer development and prognosis has been increasingly explored for predictive and prognostic biomarkers and therapeutic targets [8, 9]. Tumor-infiltrating immune cells have shown improved responses to treatment in sarcoma with prognostic consequences [10, 11]. Moreover, infiltration of lymphocytes has also been shown to determine the outcome of immunotherapy in sarcoma patients [12]. Therefore, in-depth evaluation of various TME components, particularly the tumor infiltrating immune cells, in sarcoma may reveal potential therapeutic targets for sarcoma targeted therapy.

## Material and methods

### Transcriptomic data

The training dataset utilized transcriptomic data (log<sub>2</sub> normalized FPKM [fragments per kilobase of transcript per million mapped reads]

expression values) and clinical information from soft tissue sarcoma (STS) patients (TCGA-SARC;  $n = 259$ ), sourced through the UCSC Xena browser (<https://xenabrowser.net/>). Additionally, gene expression and survival data for three supplementary sarcoma patient cohorts (GSE119041 [undifferentiated uterine sarcoma;  $n = 50$ ], GSE30929 [dedifferentiated liposarcoma;  $n = 140$ ], GSE17674 [Ewing sarcoma;  $n = 44$ ]) for external validation were acquired from the Gene Expression Omnibus (GEO) database (<https://www.ncbi.nlm.nih.gov/geo/>). The fourth cohort, TARGET OS (osteosarcoma;  $n = 88$ ), employed for further external validation. Transcriptomic data (log<sub>2</sub> normalized FPKM expression values) and clinical information for TARGET OS were also obtained from the UCSC Xena browser (<https://xenabrowser.net/>). Transcriptomic data from microarray datasets included in the present study were log<sub>2</sub> normalized using the limma R package. A summary of the datasets used in this study is outlined in Supplementary Table S1.

### TISCH analysis

The Tumor Immune Single-cell Hub (TISCH, <http://tisch.comp-genomics.org/>, accessed on 15 October 2023) is a database dedicated to evaluation of the tumor microenvironment (TME), offering cell-type annotation at the single-cell level [13]. TISCH has employed a standard pipeline in MAESTRO for preprocessing each single cell dataset [14]. In this study, we examined the gene expression levels of monocytes or macrophages (Mono/Macro) in three primary sarcoma single-cell datasets. These datasets encompassed gastrointestinal stromal tumor (GIST) (Geo accession number: GSE162115;  $N = 2$ ; single cells = 35,308), pleuropulmonary blastoma (PPB) (Geo accession number: GSE163678;  $N = 1$ ; single cells = 12,239), and synovial sarcoma (SS) (Geo accession number: GSE131309;  $N = 3$ ; single cells = 9,205).

### Tumor microenvironment annotation

Quantitative analysis of the relative abundance of 22 immune cell types in the TCGA cohort was achieved using the CIBERSORT algorithm [15]. CIBERSORT estimates immune cell proportions in bulk tissue samples using gene expression data. It relies on a reference signature matrix, LM22, derived from 570 genes that characterize the expression profiles of 22 immune cell types. By applying support vector regression, it deconvolves the mixed gene expression in tissue samples into relative contributions from each immune cell type. This method enables the inference of immune cell composition from RNA sequencing or microarray datasets. The ESTIMATE algorithm was run to eval-

uate the infiltration of stromal (stromal score) and immune cells (immune score), collectively termed the ESTIMATE score (<https://sourceforge.net/projects/estimateproject/>) [16]. The TIDE (Tumor Immune Dysfunction and Exclusion) algorithm was used to estimate the anti-tumor and immune-evasive abilities of the risk subgroups [17].

### Identification of M0-related prognostic signature

To identify the M0-related genes in sarcoma patients, we first identified significantly positively correlated genes expressed in TCGA sarcoma patients with the M0 fraction of the CIBERSORT algorithm of the TCGA SARC cohort. Significance was set at Spearman's correlation coefficient of 0.2 and a *p*-value of less than 0.01. Then, the genes differentially expressed ( $\log_{2}FC = 0.2$  and adjusted *p*-value of less than 0.05) by monocytes/macrophages in each single cell dataset were screened. A Venn diagram was created which identified 38 M0-related common differentially expressed genes (DEGs). Subsequently, we performed univariate Cox regression analysis to identify the M0-related genes with prognostic significance (*p* < 0.05). To refine and construct a robust prognostic signature, we applied multivariate Cox regression analysis. This step was crucial as it allowed us to consider the independent effect of each gene while adjusting for potential confounders, such as gene-gene correlations. The multivariate model accounts for interactions between the candidate genes, ensuring that the identified genes remain significant even in the presence of other related markers. By including multiple variables, the multivariate Cox regression narrows down the gene set to the most impactful prognostic factors. The coefficients derived from the multivariate model indicate the relative weight of each gene in predicting patient survival, allowing for a more precise risk score calculation. The risk score for each patient was then calculated based on the individual gene expression levels and their corresponding multi-Cox coefficients, employing the following formula: Risk score = (Expression of mRNA1 × Coefficient mRNA1) + (Expression of mRNA2 × Coefficient mRNA2) + ... + (Expression of mRNA<sub>n</sub> × Coefficient mRNA<sub>n</sub>).

### Risk model assessment

The classification of TCGA SARC samples into high- and low-risk subgroups was based on the median risk score. To gain insight into the spatial distribution and integration of risk within these defined groups, we employed principal component analysis (PCA), which was executed using the `prcomp` function from the R package `stats`. To assess the prognostic and predictive significance

of these risk subgroups, we used Kaplan-Meier survival analysis and generated receiver operating characteristic (ROC) curves. These analyses were carried out with the R packages `survival`, `survminer`, and `time-ROC`.

### Development of nomogram

To ascertain the independent prognostic value of the risk groups, we performed uni- and multivariate Cox regression models. Subsequently, we developed a nomogram based on the MRPS and common clinicopathological features identified through regression analysis to predict 1-, 3-, and 5-year TCGA SARC survival. The performance of our nomogram was evaluated using a calibration curve. Additionally, we conducted decision curve analysis (DCA) using the `ggDCA` package, a statistical approach that considers clinical consequences, to assess the diagnostic and prognostic value of the nomogram [18].

### Mutational landscape

Simple nucleotide variation (SNV) data of the TCGA SARC cohort were downloaded from the TCGA Data Portal (<https://portal.gdc.cancer.gov/repository/>). The oncoplot was constructed using the R package `maftools` to analyze the number and categories of gene mutations in two MRPS risk subgroups.

### Gene set enrichment analysis

Gene set enrichment analysis (GSEA) was carried out to detect enrichment of the signaling pathways involved in risk groups based on the hallmark gene sets (h.all.v2022.1) (<http://gsea-msigdb.org/gsea/msigdb/>).

### Statistical analysis

Categorical variables were compared using the  $\chi^2$  test. Two or more groups were compared using Student t/Wilcoxon and ANOVA/Kruskal-Wallis tests. Survival analysis were performed using the Kaplan-Meier method with the log-rank test. Cox regression hazard models were adopted to perform univariate and multivariate factor analyses. Spearman's and Pearson's correlation tests were used to perform correlation analysis. The statistical software R v4.0.3 (<http://www.r-project.org>) was used to carry out all the statistical analyses.

## Results

### Infiltration of M0 macrophage and its prognostic impact

In order to investigate the composition of the tumor microenvironment (TME) in sarcoma pa-

tients (TCGA SARC cohort;  $n = 259$ ), we employed the CIBERSORT algorithm, which estimates the abundance of 22 types of immune cells in sarcoma cancer tissues based on the gene expression profiles as illustrated in Figures 1 A and 1 B. The M2 phenotype, resting CD4+ memory T cells, and CD8+ T cells were the top three most infiltrated immune cells in the TME (Figure 1 B). It is noteworthy that all the three phenotypes of macrophages were among the most abundant immune cells (Figure 1 B). Prognostic analysis based on Cox regression hazard models revealed that the infiltration of the majority of the immune cells was protective in nature (Figures 2 C; Supplementary Table SII). Myeloid cells (monocytes, M0 & M2 macrophages, and resting NK cells) and activated CD4+ memory T cells were identified as risky immune cells (Figure

1 C). Among them, infiltration of M0 macrophage was significantly associated with the worst prognosis (Cox test;  $p = 0.02$ ) which was also revealed in Kaplan-Meier analysis (log-rank test;  $p < 0.001$ ) (Figure 1 D; Supplementary Figure S1). Moreover, the infiltration of M0 macrophages was evident across each pathological subtype of sarcoma, as demonstrated in Figure 1 E. Overall, these results indicate that the infiltration of M0 macrophage represents a risk factor for sarcoma patients.

### Identification of M0 macrophage related transcripts

In order to elucidate the role of M0 macrophages in sarcoma, we next focused on the identification of M0 macrophage-related genes. For this purpose, we first identified three single cell datasets be-

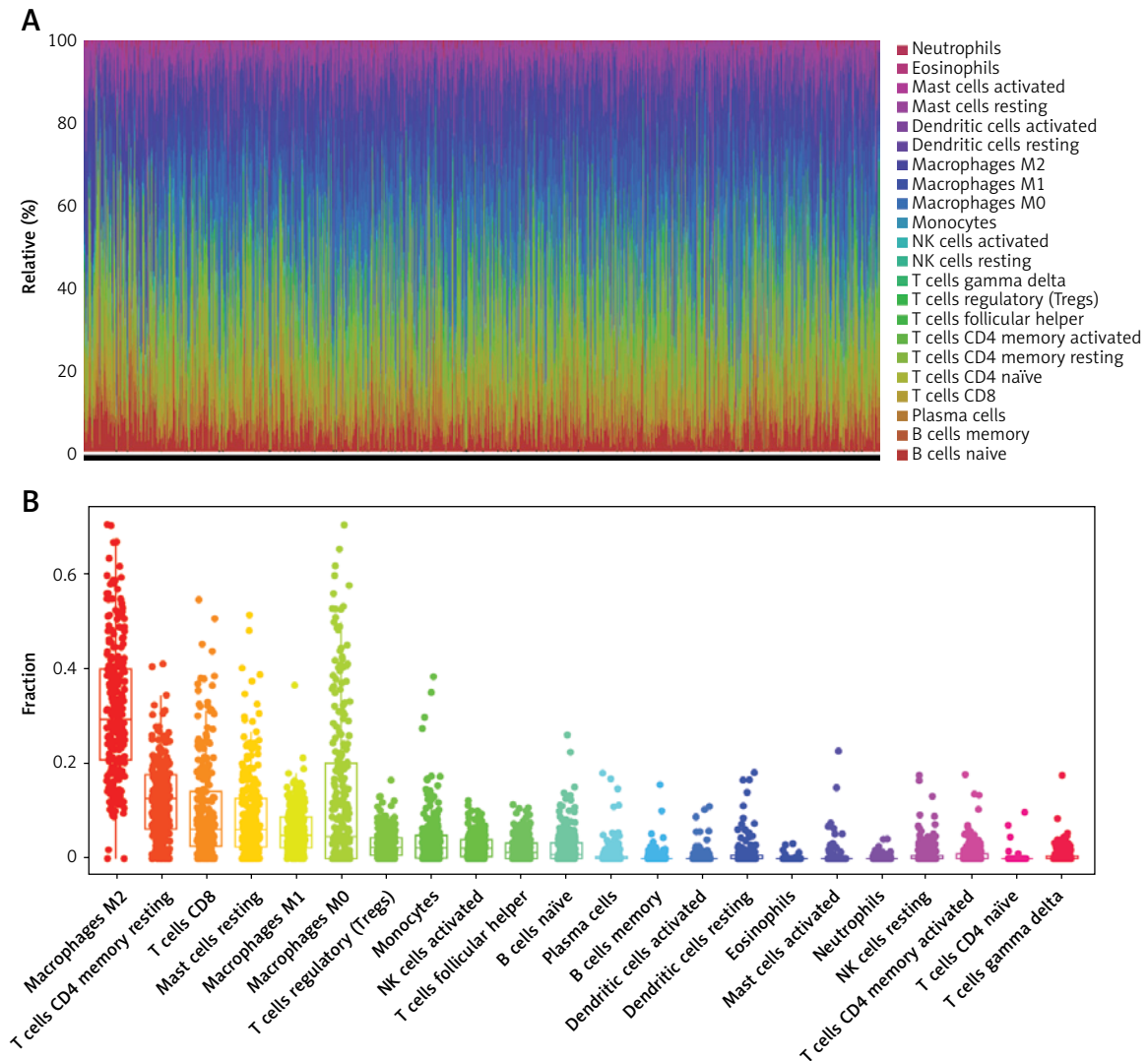


**Figure 1.** A – Heatmap of immune landscape assessed by CIBERSORT algorithm illustrating the abundance of 22 types of immune cells in sarcoma tissues. B – Bar plot presenting the infiltration fraction of 22 types of immune cells in sarcoma tissues, arranged in descending order from high to low fraction. The points represent the individual fraction value of each sample. The quartile range is illustrated as upper and lower ends of the box and the median is represented by the midline within the box

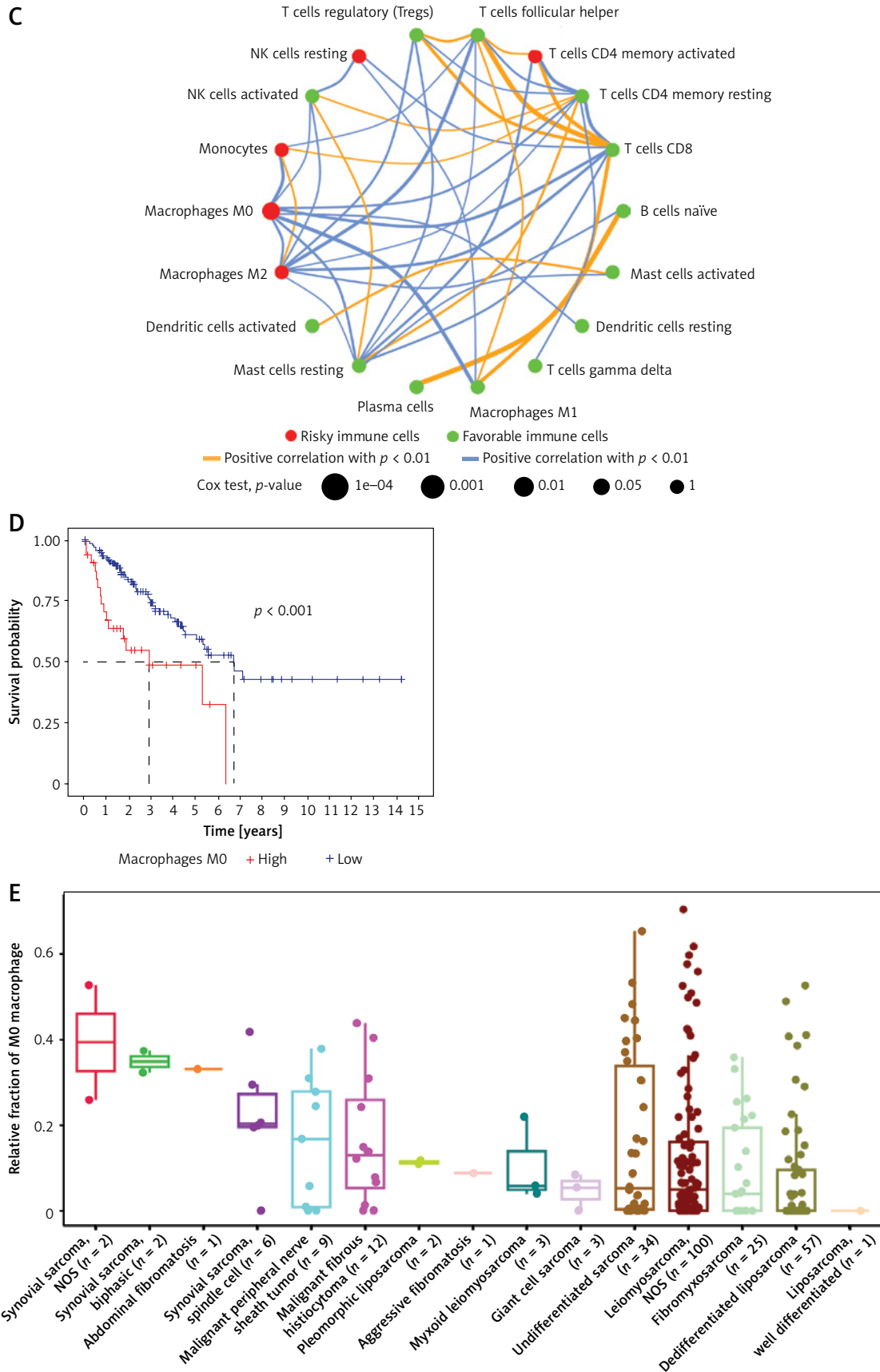


**Figure 1.** Cont. **C** – Bubble network illustrating the prognostic impact of immune cell infiltration and their inter-correlations. **D** – Kaplan-Meier survival curve showing the survival difference between sarcoma patients with or low infiltration of M0 macrophages. **E** – Bar plot illustrating the abundance of M0 macrophage in each histological type of sarcoma patients

longing to various types of sarcoma. These datasets encompassed gastrointestinal stromal tumor (GIST) (Geo accession number: GSE162115;  $N = 2$ ; single cells = 35,308), pleuropulmonary blastoma (PPB) (Geo accession number: GSE163678;  $N = 1$ ; single cells = 12,239), and synovial sarcoma (SS) (Geo accession number: GSE131309;  $N = 3$ ; single cells = 9,205). These datasets were preprocessed using the standard pipeline in MAESTRO and annotated by the TISCH team [13, 14]. All the three datasets demonstrated the infiltration of myeloid cells annotated as mono/macro cell types (Figure

2 A–C). We downloaded the DEGs (PPB = 2454; SS = 2780; GIST = 6365) between mono/macro cells in comparison to other cell types in each dataset ( $\log_{2}FC = 0.2$  and adjusted  $p < 0.05$ ). Consequently, the genes in the TCGA SARC dataset that were positively correlated ( $n = 1336$ ) with the infiltration fraction of M0 macrophages, as assessed by the CIBERSORT algorithm, were also identified (Spearman’s correlation coefficient = 0.2 and  $p < 0.01$ ; Supplementary Table SIII). The Venn diagram shows the filtering of common genes between the four datasets (Figure 2 D). A total of 38 common

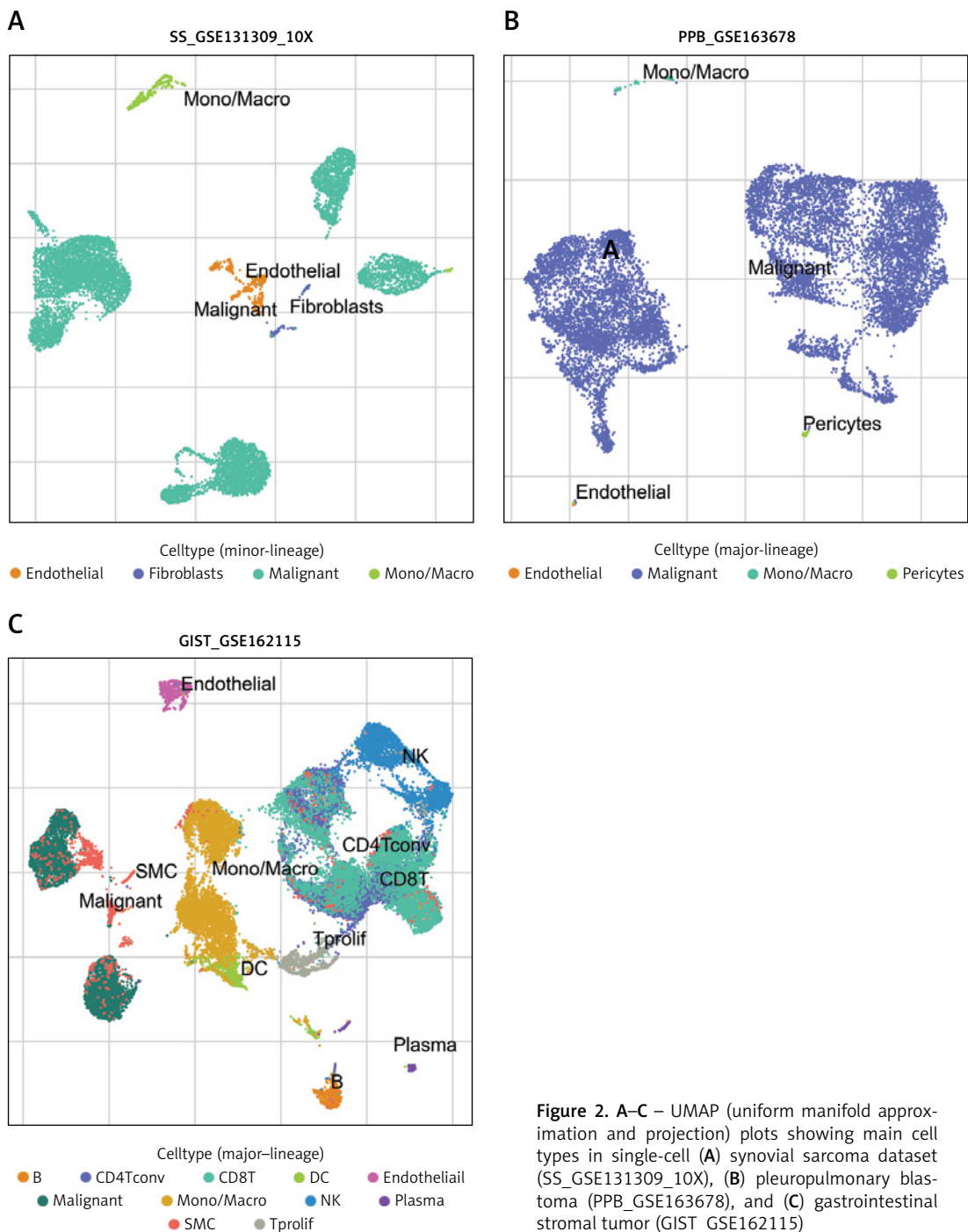


**Figure 2.** A–C – UMAP (uniform manifold approximation and projection) plots showing main cell types in single-cell (A) synovial sarcoma dataset (SS\_GSE131309\_10X), (B) pleuropulmonary blastoma (PPB\_GSE163678), and (C) gastrointestinal stromal tumor (GIST\_GSE162115)

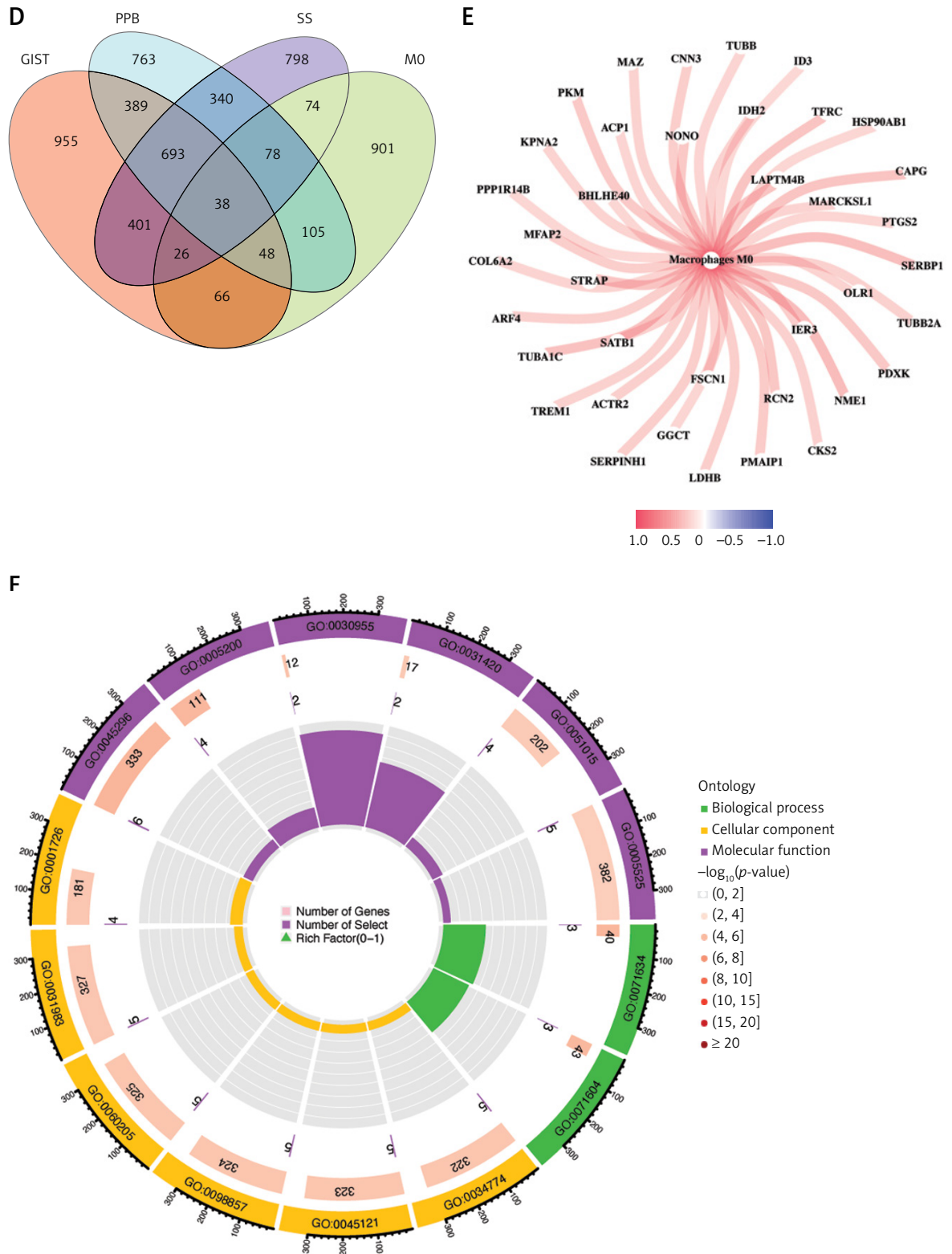


**Figure 2.** Cont. **D** – Venn diagram showing the screening of common genes among the differentially expressed genes (DEGs) by mono/macro in comparison to other cell types in the three single cell datasets and M0-related genes from the TCGA SARC dataset. **E** – Regulatory network of M0-related genes and M0 macrophages. **F** – Gene Ontology (GO) enrichment analysis of the 38 M0-related genes

genes that positively correlated with the M0 macrophages in the TCGA SARC tissues were obtained (Figure 2 E). Figure 2 F shows the enrichment of GO terms involving these genes (Supplementary Table SIII). The GO terms (GO:0071634-regulation of transforming growth factor  $\beta$  production; GO:0071604-transforming growth factor  $\beta$  production) included the production of TGF- $\beta$  as the main biological process (BP). Enriched GO terms belonging to Cellular Components (CC) indicated the involvement/association of these genes in secretion of bioactive molecules (GO:0034774-secretory granule lumen), protein folding and modification (GO:0005788-endoplasmic reticulum lumen), and intracellular trafficking and transport process (GO:0060205-cytoplasmic vesicle lumen). Molecular functions (MF) included regulation of gene expression (GO:0043425-BHLH transcription factor binding), cell adhesion (GO:0045296-cadherin binding) and structural components (GO:0005200-structural constituent of cytoskeleton and GO:0051015-actin filament binding). Moreover, these genes might also be involved in immune evasion strategies by suppressing antigen presentation (GO:0023026-MHC class II protein complex; GO:0023023-MHC class II protein complex binding) (Supplementary Table SIV). In summary, these results indicate that M0-related genes may be involved in production of TGF- $\beta$ , which is critical for tumor development and immune evasion by promoting alternative macrophage polarization and suppressing antigen presentation.

#### Establishment of M0 macrophage-related prognostic signature (MRPS)

In the next step, we aimed to identify the M0-related genes with a significant impact on prognosis, thereby augmenting their clinical relevance. The 38 M0 macrophage-related genes were subjected to univariate Cox regression analysis, which indicated 15 genes having a significant impact on sarcoma prognosis (Figure 3 A; Supplementary Table SV). Further scrutiny was performed through multivariable Cox regression analysis, which yielded 6 genes, as illustrated in Figure 3 B. A risk score, termed the M0-related prognostic signature (MRPS), was calculated for each sarcoma patient based on the multivariable Cox coefficients and mRNA expression of the genes as follows: MRPS = (0.4764  $\times$  SERBP1 expression) + (0.4133  $\times$  TUBB expression) + (0.2523  $\times$  LAPTM4B expression) + (0.2514  $\times$  SATB1 expression) + (0.2347  $\times$  ARF4 expression) + (0.1614  $\times$  MARCKSL1 expression). The distribution of risk score (MRPS) between the high and low risk as determined by the median risk score is shown in Figure 3 C. PCA showed well-separated clusters for the two MRPS subgroups, as illustrated in Figure 3 D. Patients in the MRPS-high

subgroup experienced more deaths and a shorter survival time than those in the MRPS-low subgroup (Figure 3 E). Kaplan-Meier plots of progression-free survival (PFS) and overall survival (OS) showed significantly worst survival outcomes for the MRPS-high subgroup ( $p < 0.001$ ) (Figures 3 F, G). Predictive value of the MRPS was also evaluated with time-dependent receiver operating characteristic (ROC) analysis, which showed area under the curve (AUC) values of 0.758/0.711/0.721 for 1/3/5 years in the TCGA SARC cohort (Figure 3 H).

#### Clinical and functional implications

Subsequently, we further evaluated the clinical and functional significance of the MRPS. The expression pattern of risk genes between the risk subgroups is illustrated in Figure 4 A. The MRPS-high subgroup shows high expression of the risk genes. Among the clinical features, gender, race, primary diagnosis, therapy outcome, and vital status showed significant differences in distribution between the MRPS subgroups. Female, Black, disease progression and occurrence of death were more frequent in the MRPS-high subgroup than in the MRPS-low subgroup. Since there were many small groups of patients with a unique subtype of primary diagnosis, we combined them as 'Others' and evaluated the distribution of primary diagnosis among major subtypes. The analysis revealed the abundance of leiomyosarcoma and liposarcoma in the MRPS-low subgroup and synovial and undifferentiated sarcoma in the MRPS-high subgroup ( $p = 0.007$ ) (Figure 4 B). Functional enrichment analysis of Hallmark pathways showed activation of immune response pathways in the MRPS-low subgroup, which indicates the abundance of immune cells and corresponds to the protective role of these in this subgroup. The MRPS-high subgroup, on the other hand, was enriched in oncogenic pathways and glycolysis, suggesting a high tumor component (Figure 4 C, D; Supplementary Table SVI). Moreover, the MRPS-high subgroup was also dominated by frequent mutations (71.79%) as compared to the MRPS-low subgroup (65.52%) (Figures 4 E, F). Major cancer-specific mutated genes included TP53 (35% vs. 30%), ARTX (21% vs. 8%), MUC16 (16% vs. 10%), and RB1 (12% vs. 6%). There was no difference in the occurrence of mutations in TTN (12% vs. 13%). Frameshift deletions in TP53 and ARTX were more abundant in the MRPS-high subgroup, whereas the low subgroup showed occurrence of nonsense mutations.

#### Dynamics of MRPS within sarcoma TME at single-cell level

To elucidate the dynamics of MRPS within the TME of sarcoma patients, we sought to examine

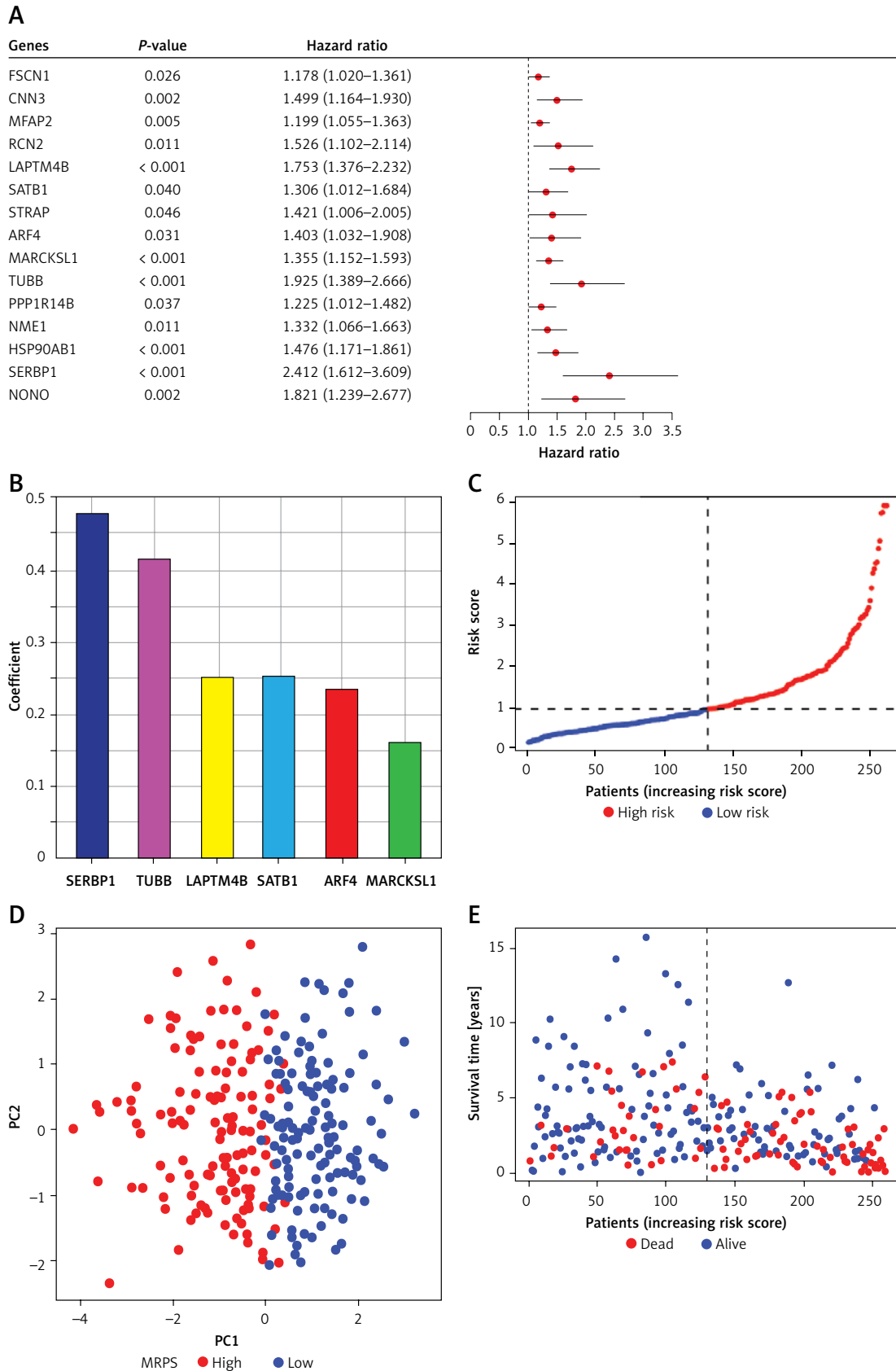


**Figure 3.** **A** – Univariate Cox regression analysis of M0-related genes. **B** – Bar plot depicting the multivariate Cox regression coefficients for each M0-related gene. **C** – Risk plot showing MRPS score on y-axis and number of patients on x-axis. **D** – Principal component analysis (PCA) plots of MRPS subgroups for TCGA SARC cohort. **E** – Risk plot of MRPS score and distribution of survival status

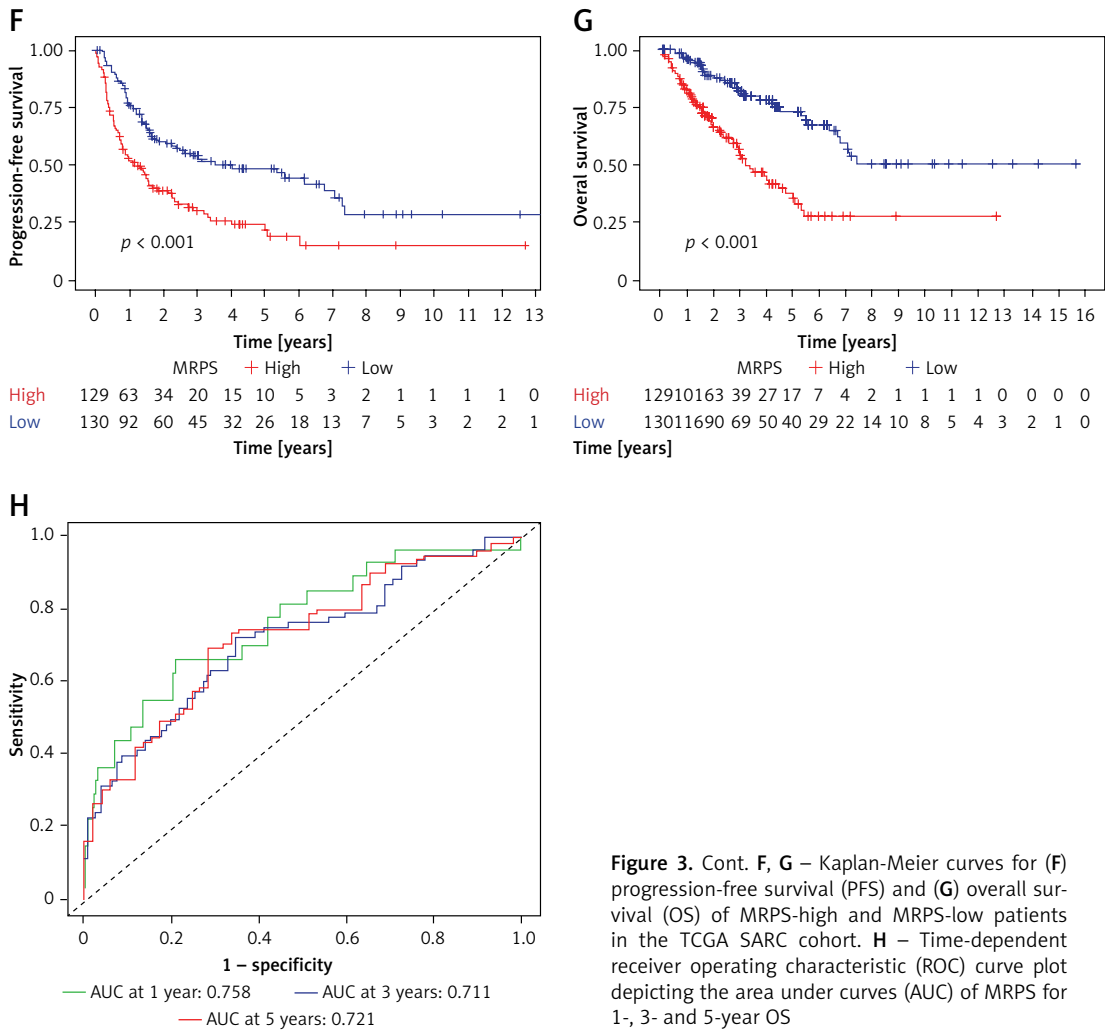


**Figure 3.** Cont. **F**, **G** – Kaplan-Meier curves for (F) progression-free survival (PFS) and (G) overall survival (OS) of MRPS-high and MRPS-low patients in the TCGA SARC cohort. **H** – Time-dependent receiver operating characteristic (ROC) curve plot depicting the area under curves (AUC) of MRPS for 1-, 3- and 5-year OS

the distribution of immune cell abundance, as determined by the CIBERSORT algorithm, across MRPS subgroups. As anticipated, the infiltration of M0 macrophages was significantly enriched in the MRPS-high subgroup (Figure 5 A). In line with the outcomes of GSEA of hallmark pathways which suggested enrichment of the inflammatory response in the MRPS-low subgroup, the MRPS-low subgroup showed enrichment of the pro-inflammatory M1 phenotype of macrophages. That also implies suppression of the M1 phenotype by MRPS risk genes. Moreover, infiltration of CD8+ T cells was higher in the MRPS-low subgroup than in the high subgroup. The majority of the immune cells were more abundant in the MRPS-low subgroup, which is also evident in the ESTIMATE results (Figure 5 B). The enrichment of MRPS was lower in immune and stromal contents as compared to tumor purity. These outcomes are fully consistent with the functional analysis described in the previous sections.

To further strengthen the reliability of these outcomes, we investigated the expression pat-

tern of MRPS signature and individual risk genes at the single-cell level. In general, the MRPS signature was significantly upregulated in malignant cells as compared to stromal and immune cells in all three datasets (Figures 5 C–H). Specifically, mono/macro annotated cells showed the lowest expression of the MRPS signature (Figure 5 C–H, Supplementary Figure S2 A). Individually, a similar pattern of expression was observed for each risk gene except LAPT4B and SATB1 (Figures 5 I–K; Supplementary Figures S2 B–E). LAPT4B showed the lowest expression in mono/macro cells while SATB1 was majorly expressed in these cells (Figures 5 I–K; Supplementary Figures S2 B–D). Hence, MRPS appears to contribute to immunosuppression in sarcoma by targeting macrophage polarization.

### Response to immunotherapy

The presence of CD8+ T cells in the TME of sarcoma patients suggests that these patients may respond to immune checkpoint therapy. However, the functional status of CD8+ T cells is important

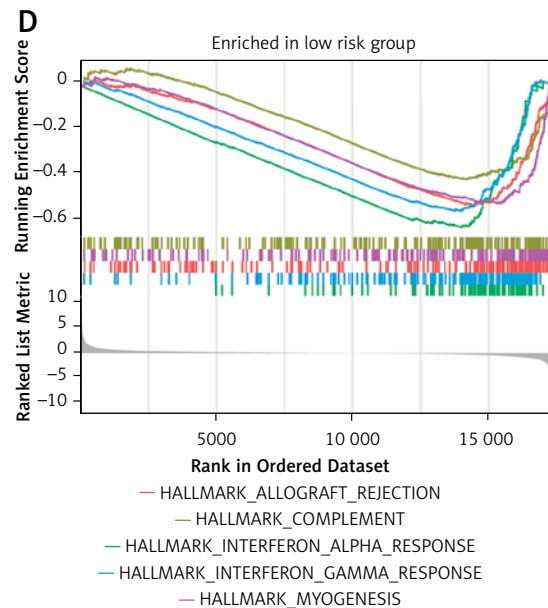
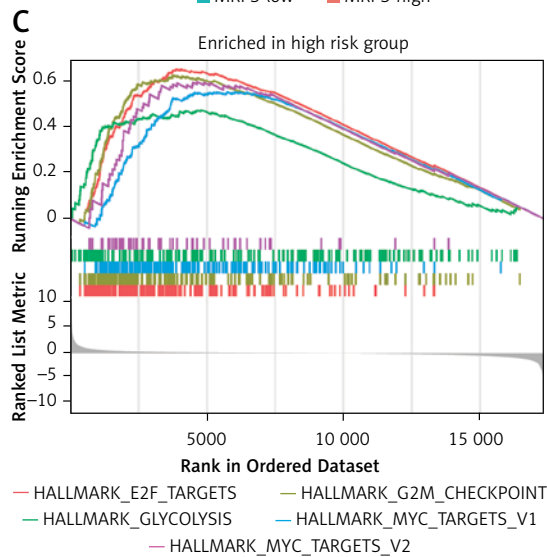
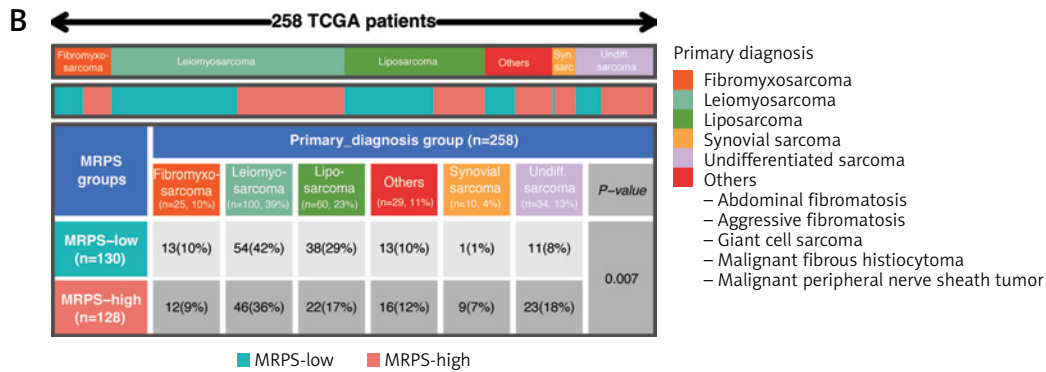
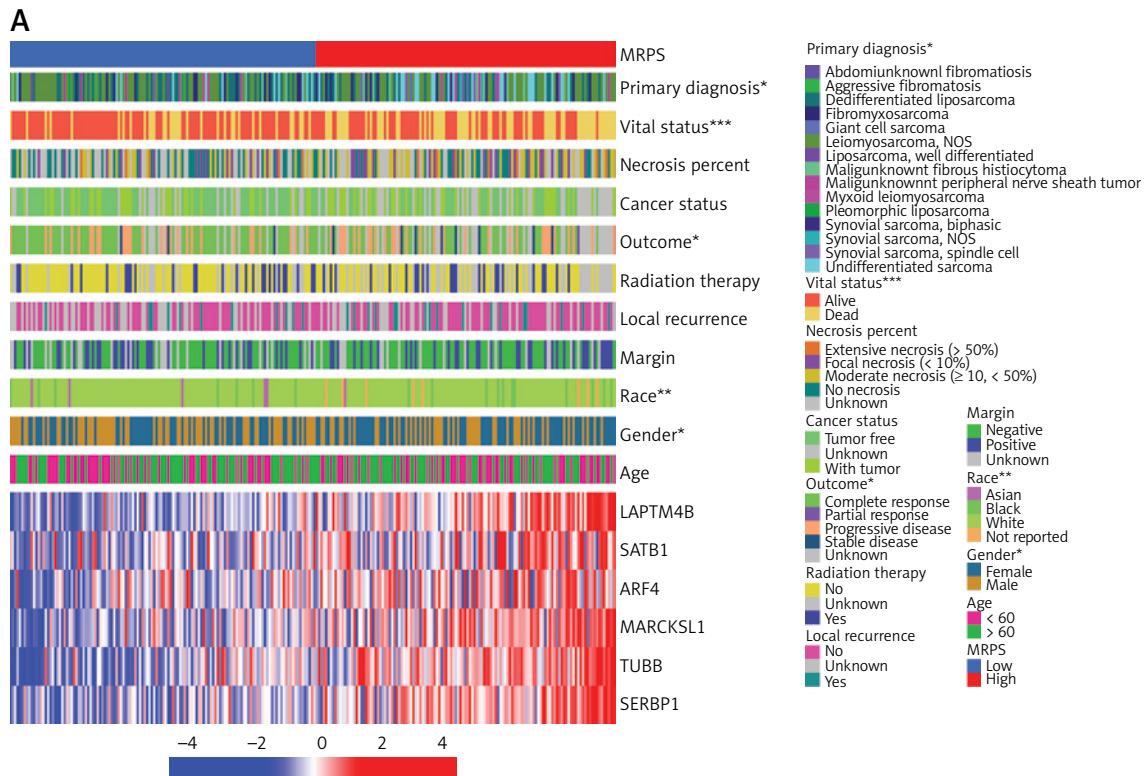


**Figure 4. A** – Heatmap illustrating the expression of 6 MRPS risk genes (red: upregulation; blue: downregulation) in the MRPS subgroups and comparison of clinicopathological features between MRPS subgroups and clinicopathological features.  $\chi^2$  test; \* $p < 0.05$ ; \*\* $p < 0.01$ ; \*\*\* $p < 0.001$ . **B** – Distribution of pathological subtypes between MRPS subgroups.  $\chi^2$  test. **C, D** – Gene Set Enrichment Analysis (GSEA) of Hallmark pathways in MRPS subgroups

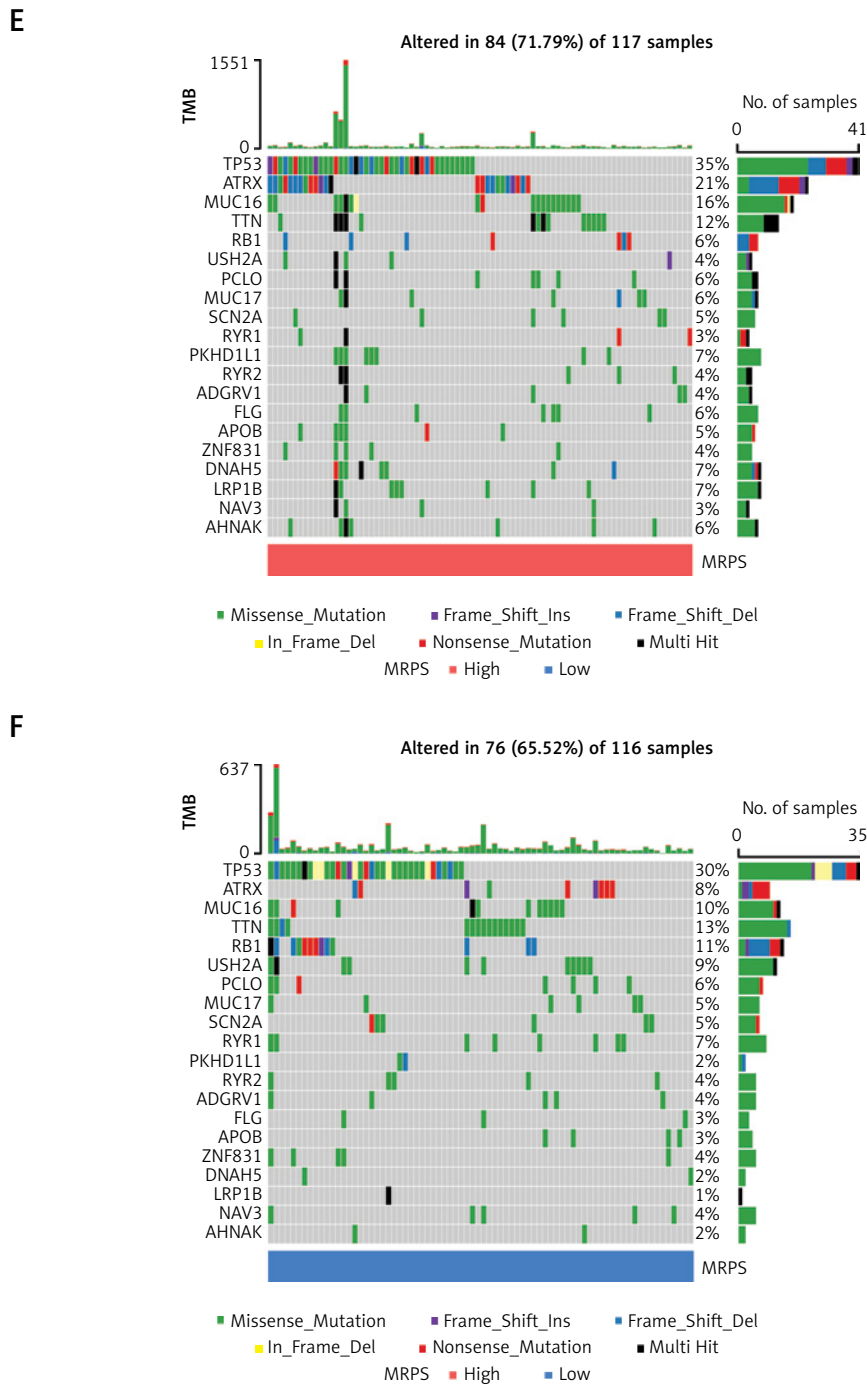


**Figure 4.** Cont. E, F – OncoPrint depicting mutation frequency of top 20 mutated genes in MRPS subgroups

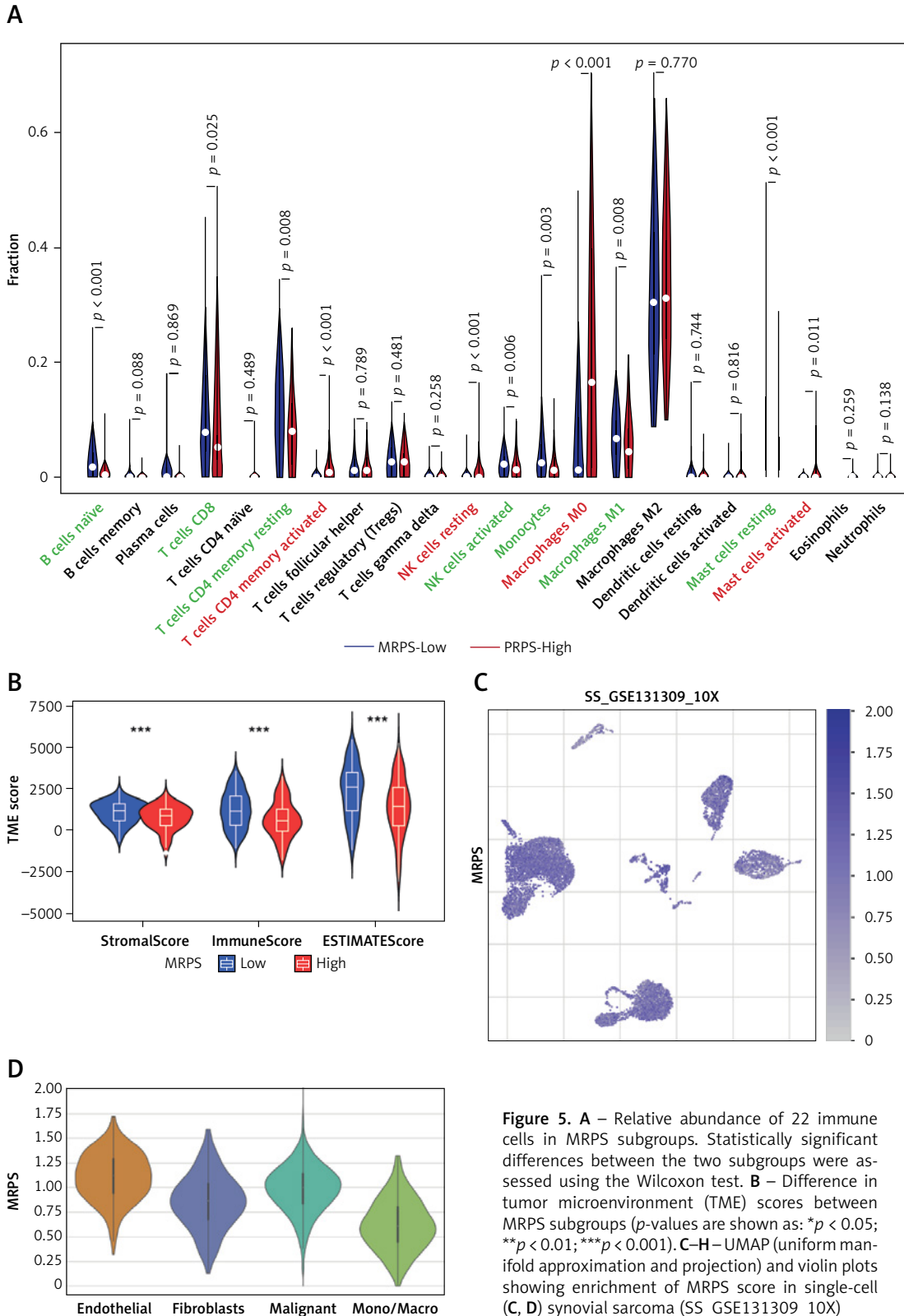
in determining whether these cells will respond or not [17]. Tumor Immune Dysfunction and Exclusion (TIDE) is a computational framework which models immune evasion strategies by cancers in terms of the T-cell dysfunction (high CTL infiltration) or exclusion (low CTL infiltration) and predicts the tumor response to ICI therapy [17]. In this cohort, the MRPS-high subgroup had high T cell exclusion and low T cell dysfunction scores (Figures 6 A–C). As such, CD8 T cells, production of interferon  $\gamma$  (IFN- $\gamma$ ), and expression of PD-L1,

mainly expressed on tumor cells and antigen presenting cells to engage CD8 T cells via PD-1/PD-L1 interaction, were lower in this cohort (Figures 6 D–F). On the other hand, only enriched presence of myeloid-derived suppressor cells (MDSC) contributed to the exclusion of T cells in the MRPS-high subgroup (Figures 6 G–I). Collectively, the TIDE score was lower for the MRPS-high subgroup, and hence 80% of the MRPS-high subgroup participants were categorized as responders (Figures 6 C, J, K).

### Validation of the MRPS in external independent sarcoma cohorts

To assess the robustness of the MRPS's applicability and limitations, survival analysis was conducted on four independent sarcoma cohorts, en-

compassing diverse histological subtypes. Within each cohort, sarcoma patients were categorized as high or low risk using the same risk estimation formula described above. This involved employing individual gene expression data in each cohort



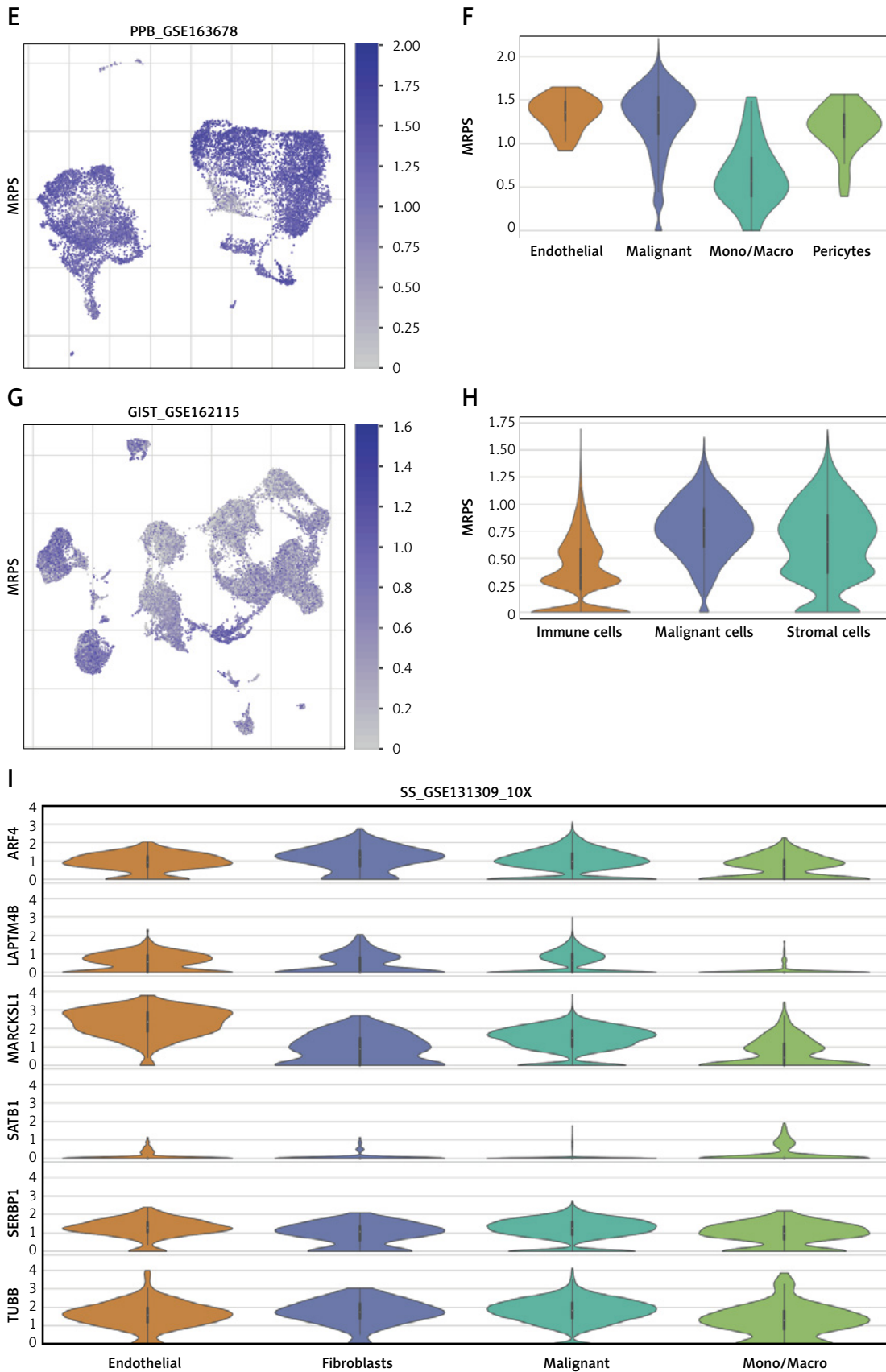


**Figure 5.** Cont. (E, F) pleuropulmonary blastoma (PPB\_GSE163678), and (G, H) gastrointestinal stromal tumor (GIST\_GSE162115) datasets. I – Violin plot showing enrichment of individual MRPS genes in each cell type in single-cell synovial sarcoma dataset (SS\_GSE131309\_10X)

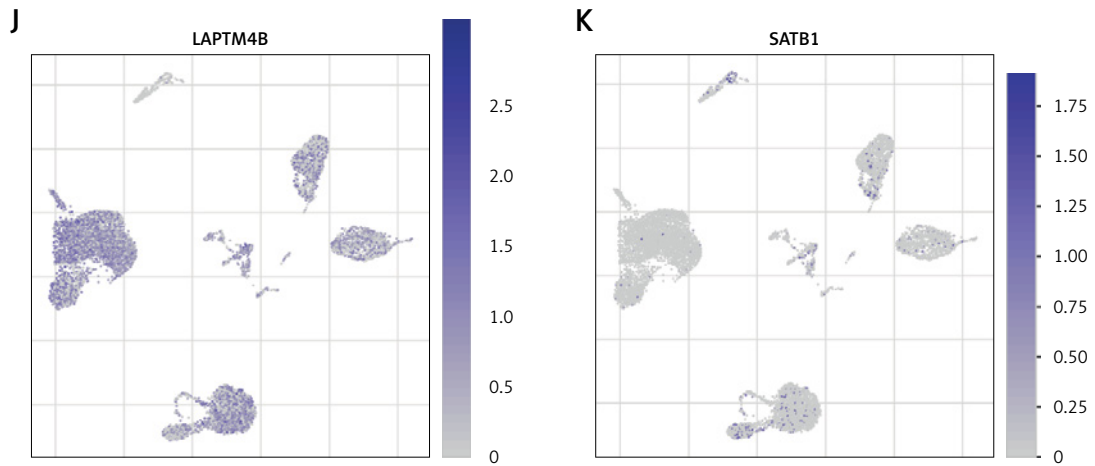


**Figure 5.** Cont. J, K – UMAP (uniform manifold approximation and projection) plots showing enrichment of (J) LAPT4B and (K) SATB1 in single-cell synovial sarcoma dataset (SS\_GSE131309\_10X)

and utilizing multivariable Cox regression coefficients derived from the TCGA SARC cohort.

The MRPS demonstrated excellent performance in cohorts where the risk signature originated, such as undifferentiated sarcoma and dedifferentiated liposarcoma (DLS) (Figures 7 A–D). Notably, risk stratification based on MRPS in 50 undifferen-

tiated uterine sarcoma (US) patients (GSE119041) revealed significantly worse survival outcomes for high-risk patients (Figure 7 A). Similarly, 140 dedifferentiated liposarcoma patients (GSE30929) exhibited the poorest disease-free survival (Figure 7 C). Receiver-operating characteristic (ROC) curve analysis also indicated comparable performance

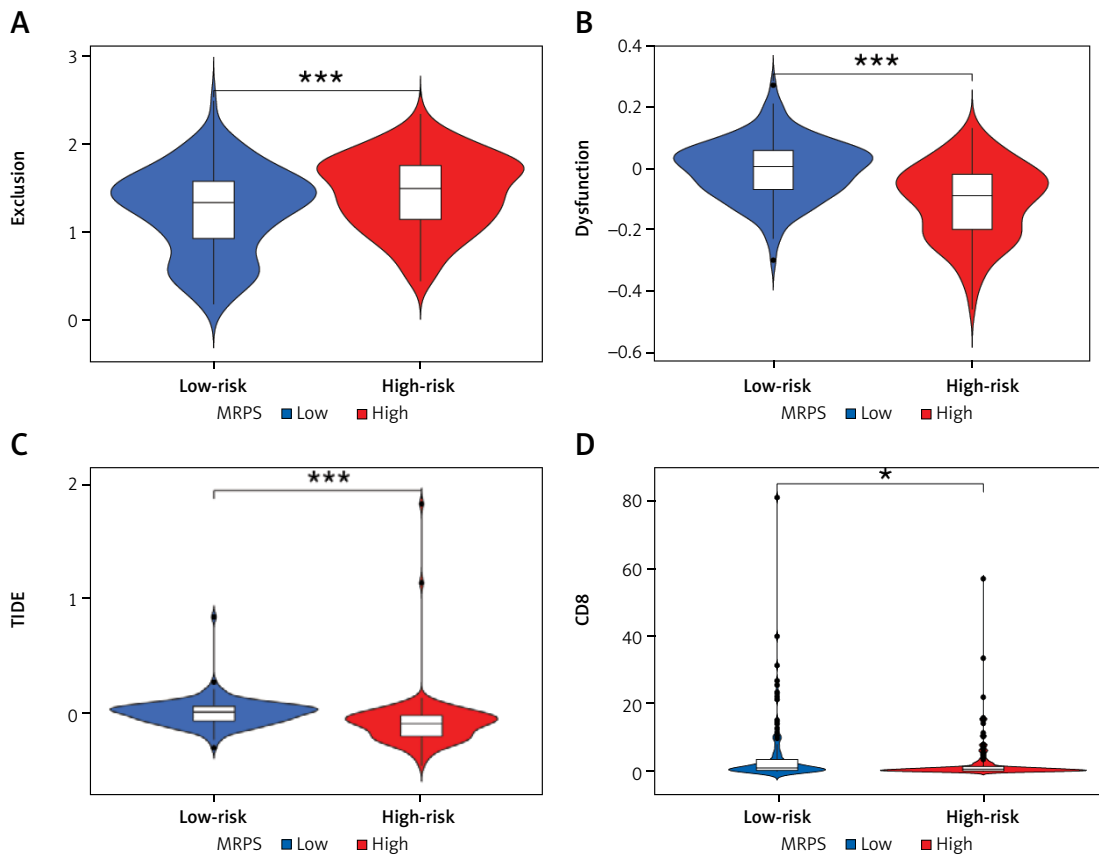


**Figure 6.** A–I – Boxplots showing comparison of Tumor Immune Dysfunction and Exclusion (TIDE) algorithm results between MRPS subgroups: A – T cell dysfunction score; B – T cell exclusion score; C – TIDE score; D – CD8. \* $p < 0.05$ ; \*\* $p < 0.01$ ; \*\*\* $p < 0.001$ ; \*\*\*\* $p < 0.0001$ ; ns – not significant

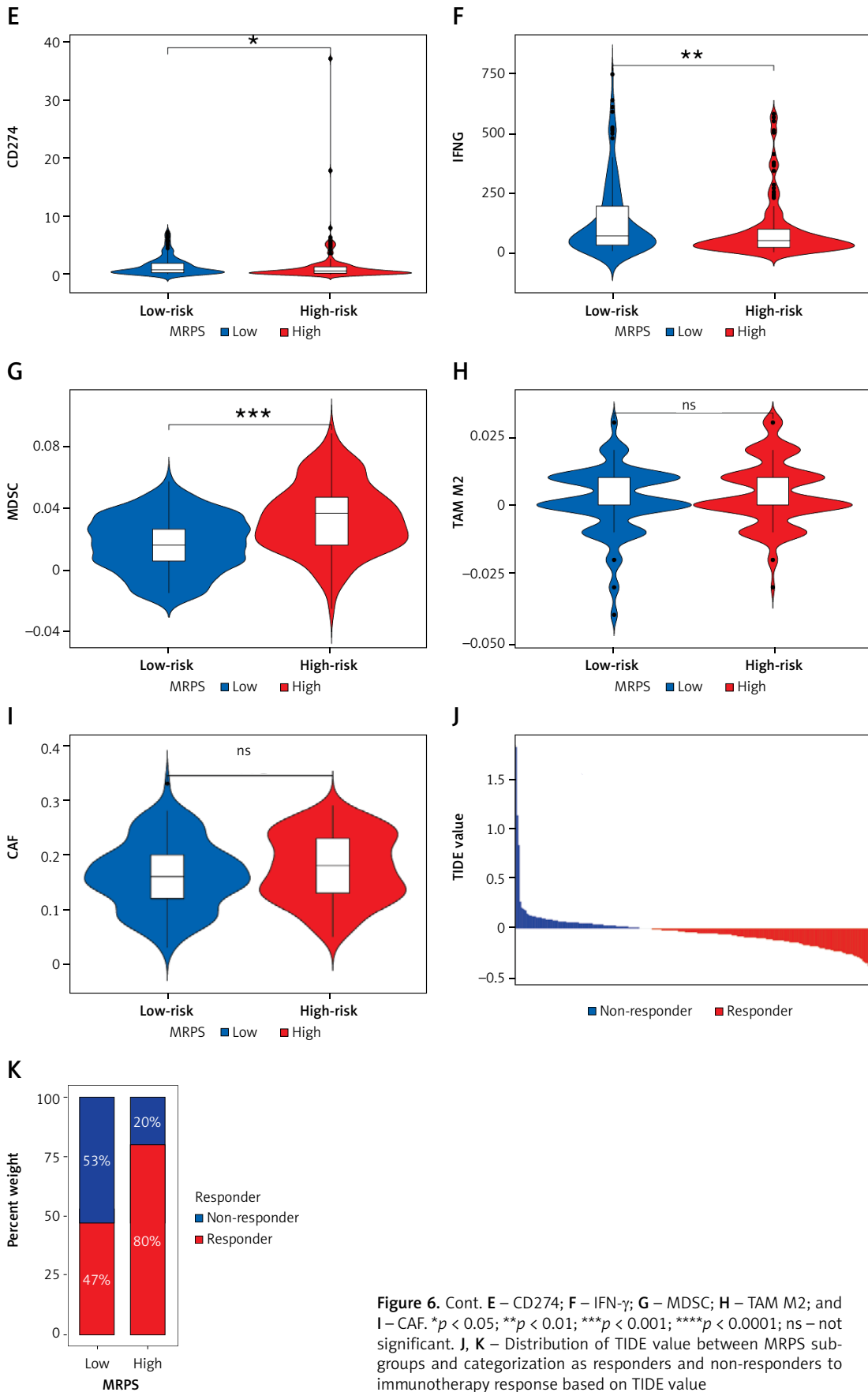


**Figure 6.** Cont. **E** – CD274; **F** – IFN- $\gamma$ ; **G** – MDSC; **H** – TAM M2; and **I** – CAF. \* $p < 0.05$ ; \*\* $p < 0.01$ ; \*\*\* $p < 0.001$ ; \*\*\*\* $p < 0.0001$ ; ns – not significant. **J, K** – Distribution of TIDE value between MRPS subgroups and categorization as responders and non-responders to immunotherapy response based on TIDE value

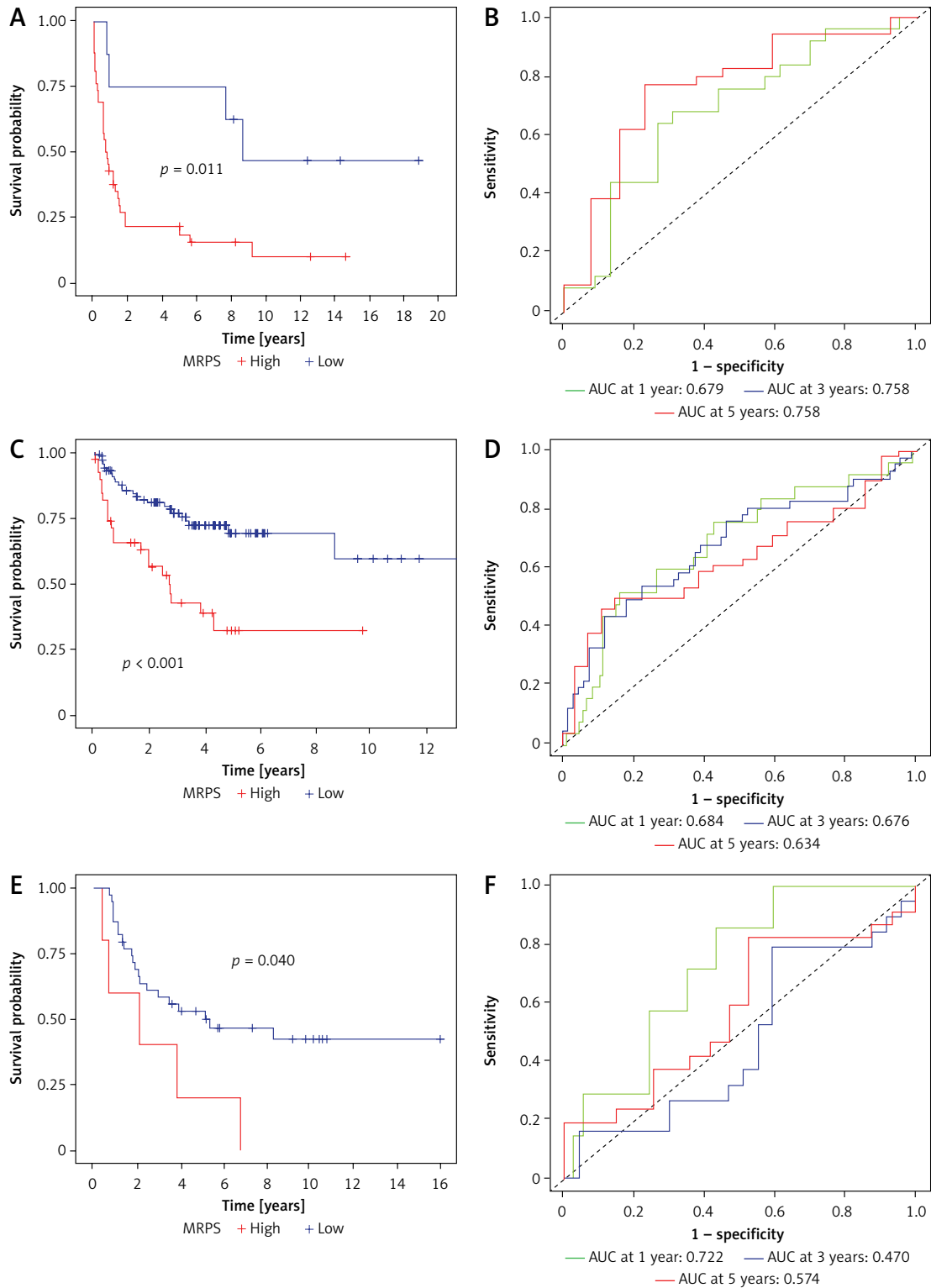


**Figure 7.** **A** – Kaplan-Meier curve for the overall survival (OS) of MRPS-stratified subgroups of undifferentiated uterine sarcoma (US) patients (GSE119041) into high- and low-risk, **B** – time-dependent receiver operating characteristic (ROC) curve plot depicting the area under the curve (AUC) of MRPS for 1-, 3- and 5-year OS. **C** – Kaplan-Meier curve for disease-free survival (DFS) of MRPS-stratified subgroups of 140 dedifferentiated liposarcoma patients (GSE30929) into high- and low-risk, **D** – time-dependent ROC curve plot depicting the AUC of MRPS for 1-, 3- and 5-year DFS. **E** – Kaplan-Meier curve for OS of MRPS-stratified subgroups of Ewing sarcoma patients (GSE17674) into high- and low-risk, **F** – time-dependent ROC curve plot depicting the AUC of MRPS for 1-, 3- and 5-year OS

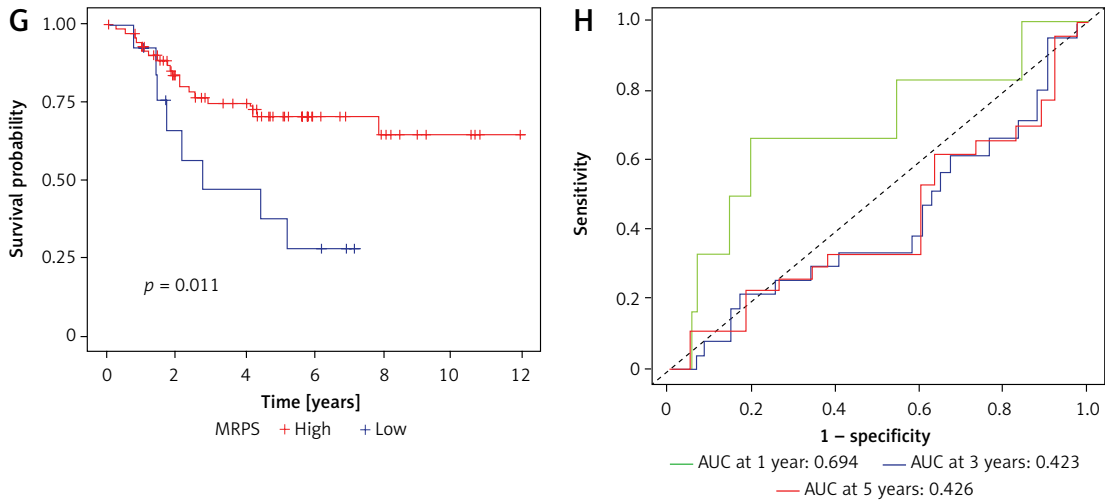


**Figure 7.** Cont. **G** – Kaplan-Meier curve for OS of MRPS-stratified subgroups of osteosarcoma patients (TARGET dataset) into high- and low-risk, **H** – time-dependent ROC curve plot depicting the AUC of MRPS for 1-, 3- and 5-year OS

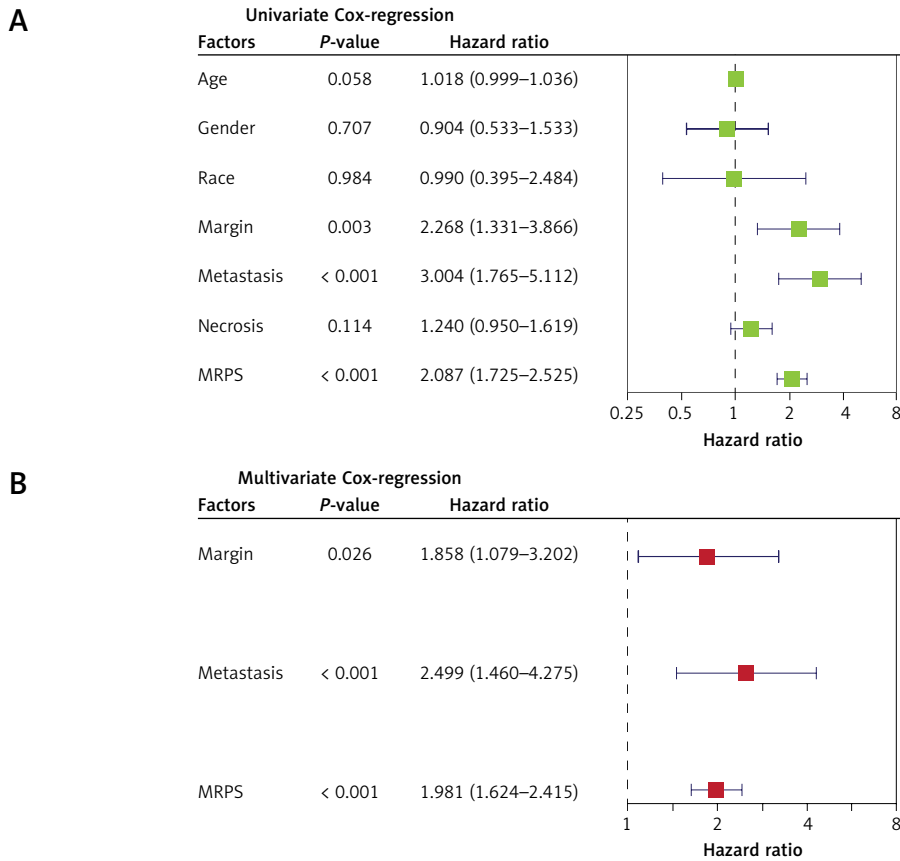


**Figure 8.** Univariate and multivariate regression analyses demonstrating independent prognostic significance of MRPS and other factors in TCGA SARC cohort

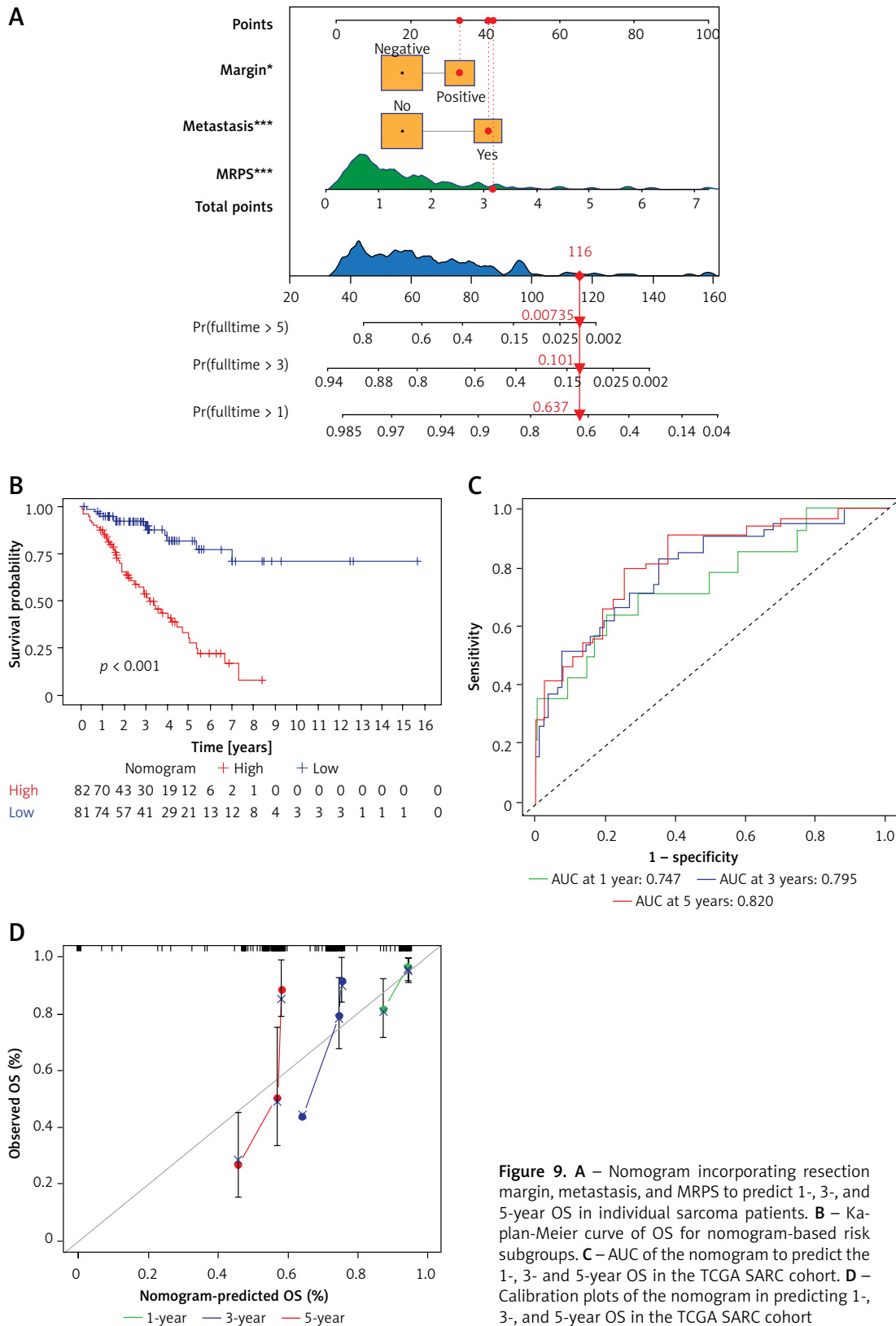


**Figure 9.** A – Nomogram incorporating resection margin, metastasis, and MRPS to predict 1-, 3-, and 5-year OS in individual sarcoma patients. B – Kaplan-Meier curve of OS for nomogram-based risk subgroups. C – AUC of the nomogram to predict the 1-, 3- and 5-year OS in the TCGA SARC cohort. D – Calibration plots of the nomogram in predicting 1-, 3-, and 5-year OS in the TCGA SARC cohort

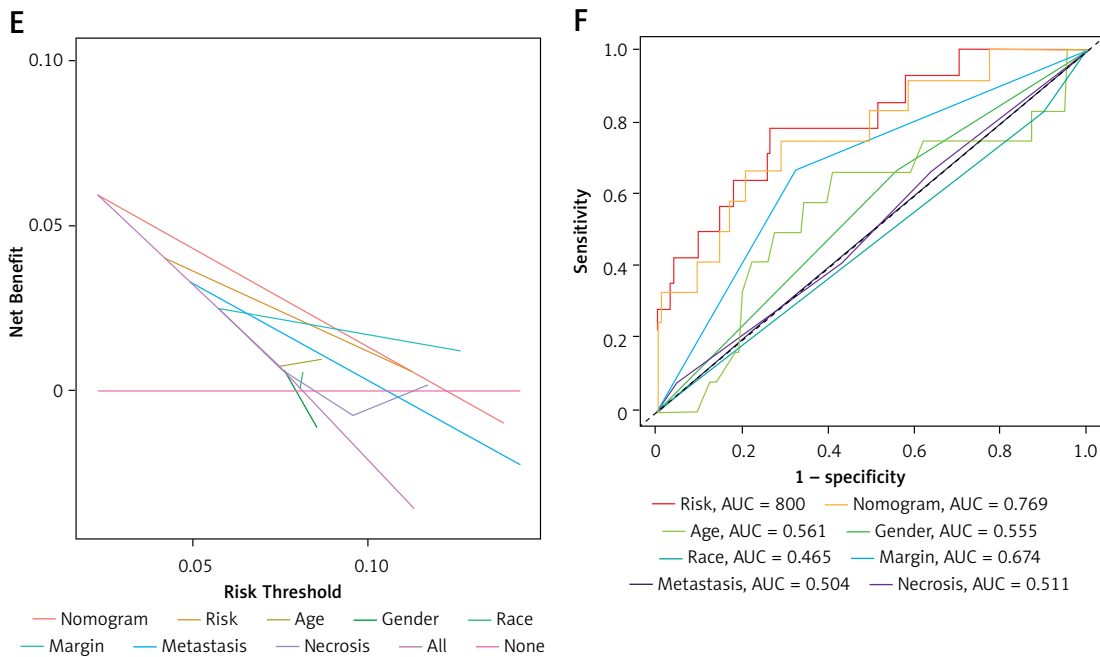


**Figure 9.** Cont. **E** – DCA (decision curve analysis) and **F** – ROC of evaluating the nomogram efficacy compared to other clinicopathological factors

to that of TCGA SARC (Figures 7 B, D). The 1-, 3-, and 5-year AUCs in the US (OS) and DLS cohorts (DFS) were 0.68/0.76/0.76 and 0.68/0.68/0.63, respectively (Figures 7 B, D).

However, MRPS performance was constrained in Ewing (GSE17674;  $n = 44$ ) and osteosarcoma (TARGET;  $n = 88$ ) patients (Figures 7 E–H). Despite a notable improvement in overall survival (OS) for Ewing sarcoma patients, only the AUC for the 1-year period exceeded 0.7 (Figures 7 E, F). Similar ROC performance was evident in osteosarcoma, with an opposite trend in OS (Figures 7 G, H). These findings suggest a more robust long-term survival predictive ability of MRPS in sarcoma subtypes from which the risk signature originated, while its effectiveness appears to be predominantly short term in other subtypes and is limited to soft-tissue sarcomas.

### Nomogram

To expand on the clinical applicability of MRPS, we constructed a nomogram incorporating the MRPS and several of the clinical features of sarcoma patients including age, gender, race, extent of necrosis, tumor resection margins, and presence of metastasis. Complete clinicopathological information was only available for 149 patients, and hence only these patients were included in the Cox regression analysis. Independent prognostic efficacy of MRPS was shown in both uni- and multivariate Cox regression analysis (Figure 8). Moreover, tumor resection margin and diagnosis of metastasis were also identified as independent

prognostic factors. Hence, these three factors were used to construct a nomogram involving 163 sarcoma patients with complete information for these two factors. Each of these factors was assigned unique points depending on its contribution to survival, as illustrated in Figure 9 A. The accumulative point scores of a single patient (highlighted as red dotted lines) with positive tumor resection margins, presence of metastasis and an MRPS score of just over 3 amounts to 116, which corresponds to 1-, 3- and 5-year survival probability of 63.7%, 10.1%, and 0.7%, respectively. Risk stratification of sarcoma patients based on the nomogram demonstrated a significant overall survival difference between high- and low-risk subgroups (Figure 9 B). The survival predictability based on ROC curves showed an enhanced performance in predicting 1-, 3-, and 5-year OS as compared to MRPS in the entire cohort (Figure 9 C). High predictive accuracy for OS was shown by the newly constructed nomogram with 1-, 3-, and 5-year AUC of 0.747, 0.795, and 0.820, respectively. Calibration plots indicate nomogram predictive ability in predicting the median 1-, 3- and 5-year OS close to observed OS values (Figure 9 D). Moreover, the decision curve analysis (DCA) demonstrated a superior benefit of the nomogram as compared to MRPS and other clinicopathological features (Figure 9 E). Moreover, MRPS (AUC = 0.800) and the nomogram (AUC = 0.769) showed similar predictive ability, which was much higher than that of other clinicopathological factors in predicting overall survival (Figure 9 F).

## Discussion

Sarcomas are a group of diverse mesenchymal neoplasms with poor prognosis [1, 6, 7]. Heterogeneity makes clinical management of sarcomas challenging due to limited applicability of current treatments across diverse subtypes [1]. Simultaneously, identification of diverse prognostic nomograms and novel therapeutics with broad applicability in this group of patients is a difficult task. Hence, exploration of avenues with a wider impact on the pathogenesis and prognosis of sarcoma is of critical importance. One such aspect is the understanding of TME features in cancer. In this study, we employed the CIBERSORT algorithm to study the dynamics of tumor-infiltrating lymphocytes and other immune cells in the TME of sarcoma patients. Overall, the presence of the various immune cells was associated with better prognosis except the M0 phenotype of macrophages. We identified a prognostic signature consisting of 6 genes related to M0 macrophages utilizing bulk and single cell RNA sequencing. The MRPS signature was proven to be an accurate prognostic parameter in 3 other external cohorts of soft-tissue sarcomas. The MRPS risk genes were mainly enriched in malignant and M0 macrophage cells, indicating a possible crosstalk parameter restricting macrophage polarization towards M1 phenotype, a pro-inflammatory phenotype. The MRPS was significantly correlated with response to immunotherapy. A nomogram was constructed to quantify individual risk assessment based on the MRPS score, which showed excellent predictive ability for overall survival of soft-tissue sarcoma patients.

It is well known that histologic grade and tumor size are important prognostic factors for local recurrence, distant metastasis, and overall survival, and there have been several attempts to develop predictive nomograms involving these clinical features [19, 20]. The Memorial Sloan Kettering Sarcoma nomogram used tumor grade, depth, size, margin status, age, and histology to predict 3- and 5-year local recurrence risk of non-metastatic sarcoma in patients who had been treated with surgery alone between 1982 and 2006 [19]. Age, tumor size, FNCLCC (Fédération Nationale des Centres de Lutte Contre le Cancer) grade, and histologic subtype were used by another team to develop two nomograms predicting overall survival and distant metastasis for sarcoma patients treated between 1994 and 2013, which were validated on three external independent cohorts [20]. Our cohort, which comprised only 149 patients with complete clinicopathological information, revealed tumor resection margin and metastasis as significant prognostic factors in univariate and multivariate Cox regression analysis. This cohort

lacked important information such as tumor size and grade, and the histologic subtypes were diverse, with a small number of participants. Hence, these factors were not included in the analysis. Age and the extent of necrosis did not show any prognostic impact, probably due to low number of participants in comparison to previous studies [19, 20]. Nonetheless, our study incorporates the resection margin and presence of metastasis as prognostic factors, which had not been previously incorporated in such nomograms. Moreover, this nomogram also used computational gene signature associated with macrophages (MRPS), which has not been reported before. Similar, computational signature-based nomograms that were derived from TME features have previously been reported [21, 22]. However, these studies utilized the ssGSEA or ImmucellAI database to identify the immune-related risk signatures (immune-related genes – IRGs), which greatly differ in composition of immune cells from the CIBERSORT database. In the study by Ren *et al.*, the risk subgroups identified lacked any significant differences in the abundance of macrophages between them as assessed by ImmucellAI, which does not probe the various macrophage phenotypes [21]. The high-risk subgroup in the study by Xiao *et al.*, however, had more M0 macrophages, but the IRG that differentiated between the three risk-subgroups was not derived from M0 macrophages and the participants were osteosarcoma patients [22]. These differences greatly differentiate our risk signature and nomogram from the previous ones.

Sarcoma exhibits the highest relative percentage of gene amplifications, deletions, and fusions, along with the lowest average mutation count compared to other tumor types [3, 23]. Genomic alterations in major tumor suppressor genes, such as TP53, RB1, and ARTX, are frequently observed in sarcoma patients and are associated with a poor prognosis [23]. Additionally, different histological subtypes of sarcoma vary in their susceptibility to genomic alterations in terms of type and frequency. For instance, in a cohort of 8000 soft tissue sarcoma (STS) patients, RB1 (22%) and CDKN2A (22%) were identified as the most commonly altered genes, leading to loss of DNA copy number and point mutations [23]. The study also suggested that CDKN2A could serve as a prognostic factor and is rarely aberrant in leiomyosarcomas and liposarcomas ( $\leq 10\%$ ). Another study focusing on 67 leiomyosarcomas revealed that ARTX was the most frequently mutated gene following TP53 and RB1 [24]. In our TCGA SARC cohort, predominantly composed of leiomyosarcomas, liposarcomas, and undifferentiated sarcoma, TP53 (35% vs. 30%), ARTX (21% vs. 8%), and RB1 (12% vs. 6%) emerged as the most frequently mu-

tated genes, with a higher frequency observed in the MRPS-high subgroup. Frameshift deletions in TP53 and ARTX were more prevalent in the MRPS-high subgroup, while the low subgroup exhibited higher occurrence of nonsense mutations.

In this study we identified six oncogenes that were mainly expressed by malignant sarcoma cells showing a positive correlation with M0 macrophages. The oncogenic role of these genes was also evident in external datasets indicating robustness of these genes in sarcoma development and prognosis. Lysosomal-associated transmembrane protein 4B (*LAPTM4B*), which was first cloned in hepatocellular carcinoma (HCC) cells, has shown upregulation in various cancers such as non-small cell lung cancer (NSCLC), osteosarcoma, breast, colorectal, gastric, pancreatic, cervical, ovarian, and prostate cancers [25–34]. Its overexpression has been shown to promote tumor growth and proliferation, invasion and metastasis [35–37]. It exerts its oncogenic effects via autophagy initiation and inhibition of apoptosis [35, 38, 39]. Another risk gene, ADP-ribosylation factor 4 (ARF4), was identified as a novel anti-apoptotic gene in human glioblastoma-derived U373MG cells [40]. ARF4 was also shown to promote cancer proliferation and migration in lung adenocarcinoma, ovarian cancer and breast cancer [41–43]. The tubulin  $\beta$  class I gene (TUBB) is overexpressed in several cancers with diverse roles in tumorigenesis [44]. TUBB acts as a structural component of microtubules, which are an essential component of cell division and transport, by forming a dimer with  $\alpha$ -tubulin [45, 46]. The MRPS high-risk subgroup had higher tumor components and was enriched in cell division activity, indicating the oncogenic role of TUBB in sarcoma development and prognosis.

A constituent of the MARCKS family, MARCKS like 1 (MARCKSL1) functions as a protein kinase C (PKC) substrate and actin binding protein [47]. MARCKSL1 modulates cytoskeletal actin dynamics and vesicular trafficking after being translocated to the cytosol upon phosphorylation by PKC or binding to calcium-dependent calmodulin. MARCKSL1 is significantly upregulated in various cancers including breast cancer, lung adenocarcinoma, esophageal squamous cell carcinoma, muscle-derived cancer, and uterine cancer [48–51]. It has been reported to be mainly involved in cancer cell invasion and migration [48, 49, 51].

SERBP1 (plasminogen activator inhibitor 1 RNA-binding protein) is a member of the RNA-binding proteins (RBPs) which serve as master regulators of gene expression. SERBP1 has been identified as a new oncogenic factor in glioblastoma with a significant impact on the production of methionine levels linking epigenetics and cancer metabolism [52]. It has also been demonstrated to promote EMT transformation

and metastasis in HCC and prostate cancer [53, 54]. Special AT-rich sequence binding protein 1 (SATB1), a chromatin organizer and transcription factor, acts as an oncogene by regulating essential cellular processes (such as differentiation, proliferation and apoptosis) through gene expression, and its increased expression is consistently associated with poor prognosis across various cancers [55, 56]. Its overexpression in cancer-associated dendritic cells was demonstrated to drive tumor-promoting activities [57]. Our single cell analysis indicated that its expression might be limited to macrophages in sarcoma and could be targeted as a direct macrophage-related target for further investigation.

Tumor-associated macrophages (TAMs) play a pivotal role in the TME of various cancers including sarcoma, where they promote cancer progression by enhancing cell proliferation, angiogenesis, metastasis, immune evasion, and therapy resistance [58–61]. This is primarily driven by their polarization into an immunosuppressive, M2-like phenotype. However, TAMs also possess antitumor capabilities, including phagocytosis and immune activation, making them dual players in cancer biology and valuable targets for therapeutic strategies [62, 63]. Approaches to modulate TAMs include reprogramming their polarization, blocking their recruitment, and targeting critical pathways [64, 65]. For example, miRNA-loaded extracellular vesicles (iEV-214) have been shown to suppress X-box binding protein 1 (XBP1), a regulator of immune dysregulation, effectively reducing TAM-mediated immunosuppression [66]. Additionally, TAMs contribute to resistance against immune checkpoint therapy by expressing molecules such as PDL1, PDL2, and VISTA, which suppress CD8+ T cell and NK cell activity [67]. Targeting these checkpoints can restore immune function and enhance antitumor responses. Our results reveal that macrophages are a prominent TME component in sarcoma, with M0 macrophages correlating with poor prognosis [60, 61]. A six-gene prognostic signature (MRPS) was identified in our study, highlighting its prognostic relevance. MRPS risk genes are predominantly enriched in malignant cells and M0 macrophages, suggesting a crosstalk that hinders polarization toward the pro-inflammatory M1 phenotype. Targeting these genes holds potential for restoring macrophage polarization and enhancing anti-cancer immunotherapy. Notably, our evaluation also suggested that the MRPS high-risk subgroup could benefit from immune checkpoint blockade, further supporting its clinical significance.

In general, the individual characterization of MRPS risk genes suggests their participation in the growth of cancer cells by directly influencing oncogenic pathways such as autophagy and apop-

tosis. These genes also contribute to metastasis through the mediation of structural regulators. Additionally, there is evidence of gene expression regulation, either promoting metastasis through enhanced metabolism or suppressing anti-cancer immunity by inhibiting antigen presentation. Further investigations into their molecular interactions and potential therapeutic interventions may pave the way for more targeted and effective treatments in the ongoing battle against cancer.

In conclusion, infiltration of immune cells in the TME of sarcoma patients was associated with better prognosis, except in the case of M0 macrophages. A six-gene prognostic signature, termed MRPS, was identified that was significantly positively correlated with M0 macrophages. These genes may exert a significant impact on the polarization of macrophages, particularly the classically activated M1 polarization, which needs further exploration. The MRPS-stratified high-risk subgroup showed enriched tumor content as demonstrated by upregulation of oncogenic pathways and glycolysis and high frequency of mutations.

Robustness of the MRPS was demonstrated in external soft-tissue sarcoma patients. A nomogram based on the MRPS was developed, serving as a reliable and practical predictive tool for identifying high-risk sarcoma patients with lower survival probabilities. Additionally, the MRPS signature exhibited promising potential in predicting the immunotherapy response, suggesting its utility in enhancing the effectiveness of personalized immunotherapy for sarcoma patients.

#### Availability of data and materials

The datasets supporting the conclusions of this article are available in the TCGA (The Cancer Genome Atlas) repository [<https://portal.gdc.cancer.gov/>] and Gene Expression Omnibus (GEO) [<https://www.ncbi.nlm.nih.gov/geo/>]. Further information and requests for resources should be directed to and will be fulfilled by the Lead Contact, Hong Lu (471739847@qq.com).

#### Funding

No external funding.

#### Ethical approval

Not applicable.

#### Conflict of interest

The authors declare no conflict of interest.

#### References

- Fletcher CDM, Bridge JA, Hogendoorn PCW, Mertens F, editors. WHO Classification of Tumours of Soft Tissue and Bone. 4th ed. Lyon, France: IARC Press, International Agency for Research on Cancer; 2013.
- Siegel RL, Miller KD, Wagle NS, Jemal A. Cancer statistics, 2023. *CA Cancer J Clin* 2023; 73: 17-48.
- Damerell V, Pepper MS, Prince S. Molecular mechanisms underpinning sarcomas and implications for current and future therapy. *Signal Transduct Target Ther* 2021; 6: 246.
- von Mehren M, Kane JM, Agulnik M, et al. Soft Tissue Sarcoma, Version 2.2022, NCCN Clinical Practice Guidelines in Oncology. *J Natl Compr Canc Netw* 2022; 20: 815-33.
- Bleloch JS, Ballim RD, Kimani S, et al. Managing sarcoma: where have we come from and where are we going? *Ther Adv Med Oncol* 2017; 9: 637-59.
- Meyer M, Seetharam M. First-line therapy for metastatic soft tissue sarcoma. *Curr Treat Options Oncol* 2019; 20: 6.
- Carbonnaux M, Brahmi M, Schiffler C, et al. Very long-term survivors among patients with metastatic soft tissue sarcoma. *Cancer Med* 2019; 8: 1368-78.
- Wang Q, Shao X, Zhang Y, et al. Role of tumor microenvironment in cancer progression and therapeutic strategy. *Cancer Med* 2023; 12: 11149-65.
- Pandya PH, Murray ME, Pollok KE, Renbarger JL. The immune system in cancer pathogenesis: potential therapeutic approaches. *J Immunol Res* 2016; 2016: 4273943.
- Ren H, Bazhin AV, Pretzsch E, et al. A novel immune-related gene signature predicting survival in sarcoma patients. *Mol Ther Oncolytics* 2022; 24: 114-26.
- Weng W, Yu L, Li Z, et al. The immune subtypes and landscape of sarcomas. *BMC Immunol* 2022; 23: 46.
- Petitprez F, de Reyniès A, Keung EZ, et al. B cells are associated with survival and immunotherapy response in sarcoma. *Nature* 2020; 577: 556-60.
- Sun D, Wang J, Han Y, et al. TISCH: a comprehensive web resource enabling interactive single-cell transcriptome visualization of tumor microenvironment. *Nucleic Acids Res* 2021; 49: D1420-d30.
- Wang C, Sun D, Huang X, et al. Integrative analyses of single-cell transcriptome and regulome using MAESTRO. *Genome Biol* 2020; 21: 198.
- Yoshihara K, Shahmoradgoli M, Martínez E, et al. Inferring tumour purity and stromal and immune cell admixture from expression data. *Nat Commun* 2013; 4: 2612.
- Newman AM, Liu CL, Green MR, et al. Robust enumeration of cell subsets from tissue expression profiles. *Nat Methods* 2015; 12: 453-7.
- Jiang P, Gu S, Pan D, et al. Signatures of T cell dysfunction and exclusion predict cancer immunotherapy response. *Nat Med* 2018; 24: 1550-8.
- Vickers AJ, Elkin EB. Decision curve analysis: a novel method for evaluating prediction models. *Med Decis Making* 2006; 26: 565-74.
- Cahlon O, Brennan MF, Jia X, Qin LX, Singer S, Alekhtiar KM. A postoperative nomogram for local recurrence risk in extremity soft tissue sarcomas after limb-sparing surgery without adjuvant radiation. *Ann Surg* 2012; 255: 343-7.
- Callegaro D, Miceli R, Bonvalot S, et al. Development and external validation of two nomograms to predict overall survival and occurrence of distant metastases in adults after surgical resection of localised soft-tissue sarcomas of the extremities: a retrospective analysis. *Lancet Oncol* 2016; 17: 671-80.
- Ren H, Bazhin AV, Pretzsch E, et al. A novel immune-related gene signature predicting survival in sarcoma patients. *Mol Ther Oncol* 2022; 24: 114-26.

22. Xiao B, Liu L, Li A, et al. Identification and verification of immune-related gene prognostic signature based on ssGSEA for osteosarcoma. *Front Oncol* 2020; 10: 607622.
23. Bui NQ, Przybyl J, Trabucco SE, et al. A clinico-genomic analysis of soft tissue sarcoma patients reveals CDKN2A deletion as a biomarker for poor prognosis. *Clin Sarcoma Res* 2019; 9: 12.
24. Darmusey L, Pérot G, Thébault N, et al. ATRX alteration contributes to tumor growth and immune escape in pleomorphic sarcomas. *Cancers* 2021; 13: 2151.
25. Yang H, Xiong F, Qi R, et al. LAPT4B-35 is a novel prognostic factor of hepatocellular carcinoma. *J Surg Oncol* 2010; 101: 363-9.
26. Wang L, Meng Y, Zhang QY. LAPT4B is a novel diagnostic and prognostic marker for lung adenocarcinoma and associated with mutant EGFR. *BMC Cancer* 2019; 19: 293.
27. Xiao M, Jia S, Wang H, Wang J, Huang Y, Li Z. Overexpression of LAPT4B: an independent prognostic marker in breast cancer. *J Cancer Res Clin Oncol* 2013; 139: 661-7.
28. Kang Y, Yin M, Jiang W, et al. Overexpression of LAPT4B-35 is associated with poor prognosis in colorectal carcinoma. *Am J Surg* 2012; 204: 677-83.
29. Zhang H, Tian B, Yu H, Yao H, Gao Z. LAPT4B-35 protein as a potential therapeutic target in gastric cancer. *Tumor Biol* 2014; 35: 12737-42.
30. Yang Z, Senninger N, Flammang I, Ye Q, Dhayat SA. Clinical impact of circulating LAPT4B-35 in pancreatic ductal adenocarcinoma. *J Cancer Res Clin Oncol* 2019; 145: 1165-78.
31. Meng F, Luo C, Hu Y, et al. Overexpression of LAPT4B-35 in cervical carcinoma: a clinicopathologic study. *Int J Gynecol Pathol* 2010; 29: 587-93.
32. Yin M, Li C, Li X, et al. Over-expression of LAPT4B is associated with poor prognosis and chemotherapy resistance in stages III and IV epithelial ovarian cancer. *J Surg Oncol* 2011; 104: 29-36.
33. Zhang H, Wei Q, Liu R, et al. Overexpression of LAPT4B-35: a novel marker of poor prognosis of prostate cancer. *PLoS One* 2014; 9: e91069.
34. Wang ZX, Guo MY, Ren J, Li GS, Sun XG. Identification of lysosome-associated protein transmembrane-4 as a novel therapeutic target for osteosarcoma treatment. *Orthop Surg* 2020; 12: 1253-60.
35. Yang H, Xiong F, Wei X, Yang Y, McNutt MA, Zhou R. Overexpression of LAPT4B-35 promotes growth and metastasis of hepatocellular carcinoma in vitro and in vivo. *Cancer Letters* 2010; 294: 236-44.
36. Meng F, Chen X, Song H, Lou G. LAPT4B down regulation inhibits the proliferation, invasion and angiogenesis of hela cells in vitro. *Cell Physiol Biochem* 2015; 37: 890-900.
37. Liu M, Yan R, Wang J, Yao Z, Fan X, Zhou K. LAPT4B-35 promotes cancer cell migration via stimulating integrin beta1 recycling and focal adhesion dynamics. *Cancer Sci* 2022; 113: 2022-33.
38. Li Y, Zou L, Li Q, et al. Amplification of LAPT4B and YWHAZ contributes to chemotherapy resistance and recurrence of breast cancer. *Nat Med* 2010; 16: 214-8.
39. Li Y, Zhang Q, Tian R, et al. Lysosomal transmembrane protein LAPT4B promotes autophagy and tolerance to metabolic stress in cancer cells. *Cancer Res* 2011; 71: 7481-9.
40. Woo IS, Eun SY, Jang HS, et al. Identification of ADP-ribosylation factor 4 as a suppressor of N-(4-hydroxyphenyl) retinamide-induced cell death. *Cancer Lett* 2009; 276: 53-60.
41. Wu Q, Ren X, Zhang Y, et al. MiR-221-3p targets ARF4 and inhibits the proliferation and migration of epithelial ovarian cancer cells. *Biochem Biophys Res Commun* 2018; 497: 1162-70.
42. Bidkhorri G, Narimani Z, Hosseini Ashtiani S, Moeini A, Nowzari-Dalini A, Masoudi-Nejad A. Reconstruction of an integrated genome-scale co-expression network reveals key modules involved in lung adenocarcinoma. *PLoS One* 2013; 8: e67552.
43. Jang SY, Jang SW, Ko J. Regulation of ADP-ribosylation factor 4 expression by small leucine zipper protein and involvement in breast cancer cell migration. *Cancer Lett* 2012; 314: 185-97.
44. Alhammad R. Bioinformatics identification of TUBB as potential prognostic biomarker for worse prognosis in ER $\alpha$ -positive and better prognosis in ER $\alpha$ -negative breast cancer. *Diagnostics (Basel)* 2022; 12: 2067.
45. Desai A, Mitchison TJ. Microtubule polymerization dynamics. *Annu Rev Cell Dev Biol* 1997; 13: 83-117.
46. Knossow M, Campanacci V, Khodja LA, Gigant B. The mechanism of tubulin assembly into microtubules: insights from structural studies. *iScience* 2020; 23: 101511.
47. El Amri M, Fitzgerald U, Schlosser G. MARCKS and MARCKS-like proteins in development and regeneration. *J Biomed Sci* 2018; 25: 43.
48. Wang J, Jarrett J, Huang CC, Satcher RL Jr, Levenson AS. Identification of estrogen-responsive genes involved in breast cancer metastases to the bone. *Clin Exp Metastasis* 2007; 24: 411-22.
49. Liang W, Gao R, Yang M, et al. MARCKSL1 promotes the proliferation, migration and invasion of lung adenocarcinoma cells. *Oncol Lett* 2020; 19: 2272-80.
50. Karagoz K, Lehman HL, Stairs DB, Sinha R, Arga KY. Proteomic and metabolic signatures of esophageal squamous cell carcinoma. *Curr Cancer Drug Targets* 2016.
51. Björkblom B, Padzik A, Mohammad H, et al. c-Jun N-terminal kinase phosphorylation of MARCKSL1 determines actin stability and migration in neurons and in cancer cells. *Mol Cell Biol* 2012; 32: 3513-26.
52. Kosti A, de Araujo PR, Li WQ, et al. The RNA-binding protein SERBP1 functions as a novel oncogenic factor in glioblastoma by bridging cancer metabolism and epigenetic regulation. *Genome Biol* 2020; 21: 195.
53. Guo K, Zheng S, Xu Y, Xu A, Chen B, Wen Y. Loss of miR-26a-5p promotes proliferation, migration, and invasion in prostate cancer through negatively regulating SERBP1. *Tumour Biol* 2016; 37: 12843-54.
54. Wang T, Xu L, Jia R, Wei J. MiR-218 suppresses the metastasis and EMT of HCC cells via targeting SERBP1. *Acta Biochim Biophys Sin* 2017; 49: 383-91.
55. Sunkara KP, Gupta G, Hansbro PM, Dua K, Bebawy M. Functional relevance of SATB1 in immune regulation and tumorigenesis. *Biomed Pharmacother* 2018; 104: 87-93.
56. Panchal O, Wichmann G, Grenman R, et al. SATB1 as oncogenic driver and potential therapeutic target in head & neck squamous cell carcinoma (HNSCC). *Sci Rep* 2020; 10: 8615.
57. Tesone AJ, Rutkowski MR, Brencicova E, et al. Satb1 overexpression drives tumor-promoting activities in cancer-associated dendritic cells. *Cell Rep* 2016; 14: 1774-86.
58. Bied M, Ho WW, Ginhoux F, et al. Roles of macrophages in tumor development: a spatiotemporal perspective. *Cell Mol Immunol* 2023; 20: 983-92.
59. Li H, Fan J, Ma J, Qiao L, Sha T, Ma B. Exosomal miR-182-5p from breast cancer cells reprogram tumor-associated

- macrophages and promote triple-negative breast cancer progression by targeting Notch1 in macrophages. *Arch Med Sci* 2024. doi:10.5114/aoms/187080.
60. Zhang QW, Liu L, Gong CY, et al. Prognostic significance of tumor-associated macrophages in solid tumor: a meta-analysis of the literature. *PLoS One* 2012; 7: e50946.
  61. Zajac AE, Czarnecka AM, Rutkowski P. The role of macrophages in sarcoma tumor microenvironment and treatment. *Cancers* 2023; 15: 5294.
  62. Mills CD, Kincaid K, Alt JM, Heilman MJ, Hill AM. M-1/M-2 macrophages and the Th1/Th2 paradigm. *J Immunol* 2000; 164: 6166-73.
  63. Ling H, Yang Z, Sun Y, et al. The impact of diffuse large B-cell lymphoma-derived exosomes on macrophage polarisation and cytokine release. *Arch Med Sci* 2020. doi:10.5114/aoms.2020.97355.
  64. Li M, He L, Zhu J, Zhang P, Liang S. Targeting tumor-associated macrophages for cancer treatment. *Cell Biosci* 2022; 12: 85.
  65. Mantovani A, Allavena P, Marchesi F, et al. Macrophages as tools and targets in cancer therapy. *Nat Rev Drug Discov* 2022; 21: 799-820.
  66. Almanza G, Searles S, Zanetti M. Delivery of miR-214 via extracellular vesicles downregulates Xbp1 expression and pro-inflammatory cytokine genes in macrophages. *Extracell Vesicles Circ Nucl Acids* 2024; 5: 249-58.
  67. Zhou L, Zhao T, Zhang R, Chen C, Li J. New insights into the role of macrophages in cancer immunotherapy. *Front Immunol* 2024; 15: 1381225.